

Immune-mediated tubule atrophy promotes acute kidney injury to chronic kidney disease transition

Received: 8 January 2021

Accepted: 5 August 2022

Published online: 19 August 2022

 Check for updatesLeyuan Xu¹✉, Jiankan Guo¹, Dennis G. Moledina¹ & Lloyd G. Cantley¹✉

Incomplete repair after acute kidney injury can lead to development of chronic kidney disease. To define the mechanism of this response, we compared mice subjected to identical unilateral ischemia-reperfusion kidney injury with either contralateral nephrectomy (where tubule repair predominates) or contralateral kidney intact (where tubule atrophy predominates). By day 14, the kidneys undergoing atrophy had more macrophages with higher expression of chemokines, correlating with a second wave of proinflammatory neutrophil and T cell recruitment accompanied by increased expression of tubular injury genes and a decreased proportion of differentiated tubules. Depletion of neutrophils and T cells after day 5 reduced tubular cell loss and associated kidney atrophy. In kidney biopsies from patients with acute kidney injury, T cell and neutrophil numbers negatively correlated with recovery of estimated glomerular filtration rate. Together, our findings demonstrate that macrophage persistence after injury promotes a T cell- and neutrophil-mediated proinflammatory milieu and progressive tubule damage.

Acute kidney injury (AKI) is the syndromic term used to describe the abrupt reduction in glomerular filtration rate (GFR) caused by an insult such as ischemia, sepsis, nephrotoxin exposure or urinary obstruction. Based on animal models, these insults often precipitate a rapid innate immune response dominated by neutrophil and proinflammatory macrophage recruitment with significant tubular and endothelial injury, leading to GFR reduction even after correction of the inciting event^{1–6}. Under ideal conditions (e.g., transient insults in young healthy subjects), repair pathways that include neutrophil egress and a switch to reparative macrophage activation then promote clearance of cell debris and proliferation of surviving tubular cells, leading to restoration of nephron structure and GFR^{7–10}. However, in many cases this repair phase is incomplete and includes maladaptive processes such as interstitial fibrosis and tubule atrophy¹¹. As a result, people who survive AKI are at an 8.8-fold increase in risk for chronic kidney disease (CKD) and a 3.3-fold increase in risk for end stage renal disease (ESRD)^{12–14}. To date, no therapy is available to improve the post-injury repair process or prevent progression from AKI to CKD. Defining the signals that promote maladaptive kidney repair following AKI may therefore help

us identify therapeutic targets to prevent or even reverse tubule atrophy and the progression to CKD.

Investigations of animal models in which the initial injury stimulus is sustained, such as unilateral ureteral obstruction (UUO), have shown that macrophages progressively accumulate in the kidney interstitium adjacent to unrepaired tubules and promote kidney fibrosis^{15–17}. However, the underpinnings of kidney fibrosis and atrophy following transient insults, as is frequently seen in hospitalized patients, are currently unknown. In models of transient injury such as bilateral ischemia-reperfusion injury (IRI), or unilateral IRI with the contralateral nephrectomy (IRI/CL-NX), kidneys undergo a biphasic response of initial tubule cell death driven in part by an innate proinflammatory activation, followed by tubule repair and restoration of normal or near-normal function^{7–10}. However, using the model of unilateral IRI with the contralateral kidney left intact (U-IRI), we and others have shown that the injured kidney undergoes progressive atrophy and fibrosis rather than successful repair^{18–21}. These transiently injured kidneys continue to exhibit large numbers of macrophages long after the tubule repair phase is complete (days 7–10). Knock-out of either the macrophage

¹Department of Internal Medicine/Section of Nephrology, Yale University School of Medicine, New Haven, CT, USA. ✉e-mail: leyuan.xu@yale.edu; lloyd.cantley@yale.edu

survival factor chitinase 3-like 1 (*Chi3l1* or *Brp-39*) or *Ccr2*, the chemokine receptor for monocyte chemoattractant protein-1 (*Mcp1* or *Ccl2*) reduces macrophage numbers and the degree of fibrosis^{20,21}, but does not significantly impact the degree of tubule or kidney atrophy²¹. This disconnection between fibrosis and atrophy suggests that the progressive loss of kidney tubules during AKI-to-CKD transition involves mechanisms in addition to accumulation of extracellular matrix²².

To better understand the pathogenesis of AKI-to-CKD transition and specifically the mechanism of kidney tubule atrophy, we compared the kidney response to identical times of ischemic injury between mice subjected to U-IRI (to induce atrophy) or IRI/CL-NX (to induce adaptive repair). We performed single-cell-RNA-sequencing (scRNA-seq) analysis on day 7, 14, and 30 after injury to identify major cell types in the kidney and the differential transcriptional response between the models in each cell type. We confirmed our previous finding that U-IRI leads to macrophage persistence beyond the period of normal repair, and now show that those macrophages express high levels of T cell and neutrophil activating chemokines including *Cxcl16* and *Mcp2* (*Ccl8*), corresponding with a second wave of infiltrating *Cxcr6* + T cells and *Ccr1* + neutrophils in the interstitium. This late recruitment of T cells and neutrophils closely associated with a proinflammatory milieu including *Trf* and *Il1b*. Concomitantly, the tubular cells from U-IRI kidneys expressed a different profile of injury markers including vascular cell adhesion molecule 1 (*Vcam1*) and class I & II major histocompatibility (MHC) genes (rather than *Kim1*), and exhibited a dedifferentiated expression profile, correlating with late kidney atrophy. Depletion of T cells and neutrophils together, but not individually, was found to attenuate the second wave of injury and partially restore tubule mass in the U-IRI model. Consistent with the mouse models, we found that increasing numbers of T cells and neutrophils in the renal interstitium at the time of renal biopsy for AKI negatively correlated with 6-month recovery of GFR. Together, these findings suggest that failed tubule repair leads to macrophage persistence with a second wave of T-cell and neutrophil-dependent proinflammatory immune activation that induces secondary tubule injury and promotes kidney atrophy during AKI-to-CKD transition.

Results

U-IRI leads to tubule atrophy and tubule cell dedifferentiation

Phenotypically, the injured kidneys from the IRI/CL-NX mice had hypertrophied by day 7 after injury; whereas the injured kidneys from the U-IRI mice were equal in size to controls on day 7, but progressively atrophied afterwards (Fig. 1a and Supplementary Fig. 1a–c). By day 30, IRI/CL-NX kidneys weighed 38% more than age-matched control kidneys and the same as kidneys 30 days after contralateral nephrectomy alone (Supplementary Fig. 1d), while U-IRI kidneys weighed 58% less than control kidneys and 69% less than IRI/CL-NX kidneys (Fig. 1b). This resulted in a 38% and 46% decrease in cross-sectional area of the U-IRI kidneys relative to control and IRI/CL-NX kidneys, respectively (Fig. 1c). Staining for the general tubular epithelial cell marker KSP-cadherin^{23,24} revealed a 56% reduction in absolute tubular area 30 days after U-IRI as compared to IRI/CL-NX (Fig. 1d, e), however, the proportion of renal parenchymal area comprised of tubules was only 12% lower in the atrophied U-IRI kidneys than in the hypertrophied IRI/CL-NX kidneys (Fig. 1e). This suggests that kidney atrophy after AKI is predominantly due to reduced tubular mass rather than replacement of tubule epithelia by fibrosis^{20,21}. To assess the differentiation state of the remaining tubules, LTL and megalin staining were performed to quantify the area of preserved proximal tubule brush border^{25,26}. This showed that PT brush border area comprised ~29% less of the remaining renal parenchymal area 30 days after U-IRI compared to IRI/CL-NX (Fig. 1f–i). Quantitative PCR analysis for the mature proximal tubular brush border constituents megalin (*Lrp2*), NaPi-IIa (*Scl34a1*), and NaDC3

(*Scl3a3*) along with IF staining for megalin protein confirmed that proximal tubule redifferentiation was significantly reduced at 14 and 30 days in the U-IRI kidneys as compared to IRI/CL-NX kidneys (Fig. 2a–c). Of note, mice subjected to IRI/CL-NX and mice subjected to U-IRI had equivalent creatinine levels on days 14 and 30, with BUN values that approached equivalence, suggesting nearly complete recovery of filtration function by the previously injured IRI/CL-NX kidneys as compared to the uninjured kidneys in the U-IRI mice (Supplementary Fig. 1e, f).

Both mRNA and protein expression levels of the proximal tubule acute injury marker *Kim1* (*Haucr1*) were equally upregulated on day 1 after IRI in both models, confirming that the initial ischemic injury was equivalent following U-IRI and IRI/CL-NX (Fig. 2a–c and Supplementary Fig. 2)²⁷. Of note, serum levels of both KIM-1 and NGAL were significantly higher on day 1 after IRI/CL-NX than after U-IRI, likely due to clearance by the intact contralateral kidney in mice subjected to U-IRI (Supplementary Fig. 3). Serum levels of both KIM-1 and NGAL on day 1 were equivalent between survivors and non-survivors in the IRI/CL-NX mice, indicating equivalent initial injury between the surviving IRI/CL-NX and U-IRI comparison groups on days 7, 14, and 30 (Supplementary Fig. 3b, d). However, *Kim1* remained substantially higher in the kidneys subjected to U-IRI on days 7 and 14 at the mRNA level and day 14 at the protein level (Fig. 2a–c). As compared to *Kim1*, *Vcam1* was not upregulated on day 1 after IRI in either model but markedly increased afterwards, and was significantly higher in U-IRI kidneys than IRI/CL-NX kidneys from day 7 to day 30 (Fig. 2a), correlating with the period of progressive atrophy seen in this model (Fig. 1b). Together, these data suggest that tubular cells are subjected to equivalent initial ischemic injury in both models correlating with increased *Kim1* expression, followed by delayed injury and failure to redifferentiate that predominates in the U-IRI model and correlates with increased *Vcam1* expression.

Kidney atrophy is preceded by a second wave of immune activation and proximal tubule cell loss

As the difference in kidney injury marker expression between the two models became apparent on day 7 (Fig. 2a), we performed single-cell RNA sequencing (scRNA-seq) of the injured kidneys on days 7, 14, and 30 after IRI to identify the transcriptional and cellular differences underlying tubule repair and tubule atrophy. Unsupervised clustering generated twenty seven distinct cell types with gene expression profiles identifying them as proximal tubule (PT-S1, -S2, and -S3), injured PT, thick ascending limb (TAL), DCT/CNT (distal convoluted tubule/connecting tubule), collecting duct-principal cells (CD-PC), collecting duct-intercalated cells (CD-IC), endothelium, myofibroblasts, six clusters of macrophages (monocyte, infiltrating, M1, M2, proliferating, and resident macrophages), four clusters of dendritic cells [plasmacytoid DC (pDC), conventional DCs (cDC1 and cDC2), and proliferating cDC1], two clusters of neutrophils (Ngal high and low), four clusters of T cells [naïve, Cd4 + T helper/regulatory T (Th/Treg), Cd8a+ cytotoxic T/natural killer T (Tc/NKT), and proliferating T cells], and B cells (Fig. 3a, b).

The kidney atrophy seen on day 14 and 30 after U-IRI was found to correspond to a decrease in tubular cell populations relative to the total cells present, with the greatest loss occurring in the PT cell compartment beginning by day 7 (Fig. 3c, Supplementary Fig. 4, and Supplementary Table 2). Along with tubular cell loss, U-IRI kidneys exhibited an increased percentage of immune cells including macrophages, cDCs, neutrophils, and T cells as compared to the IRI/CL-NX kidneys. Of the immune cells identified, macrophages and DCs were the predominant cell types in the kidney on day 7 after injury in both models. However, both neutrophils and T-cell populations markedly increased by day 14 after U-IRI as compared to those cells in IRI/CL-NX kidneys.

Consistent with the scRNA-seq analysis, quantitative PCR of whole-kidney RNA revealed that markers for macrophages (*Adgre1*

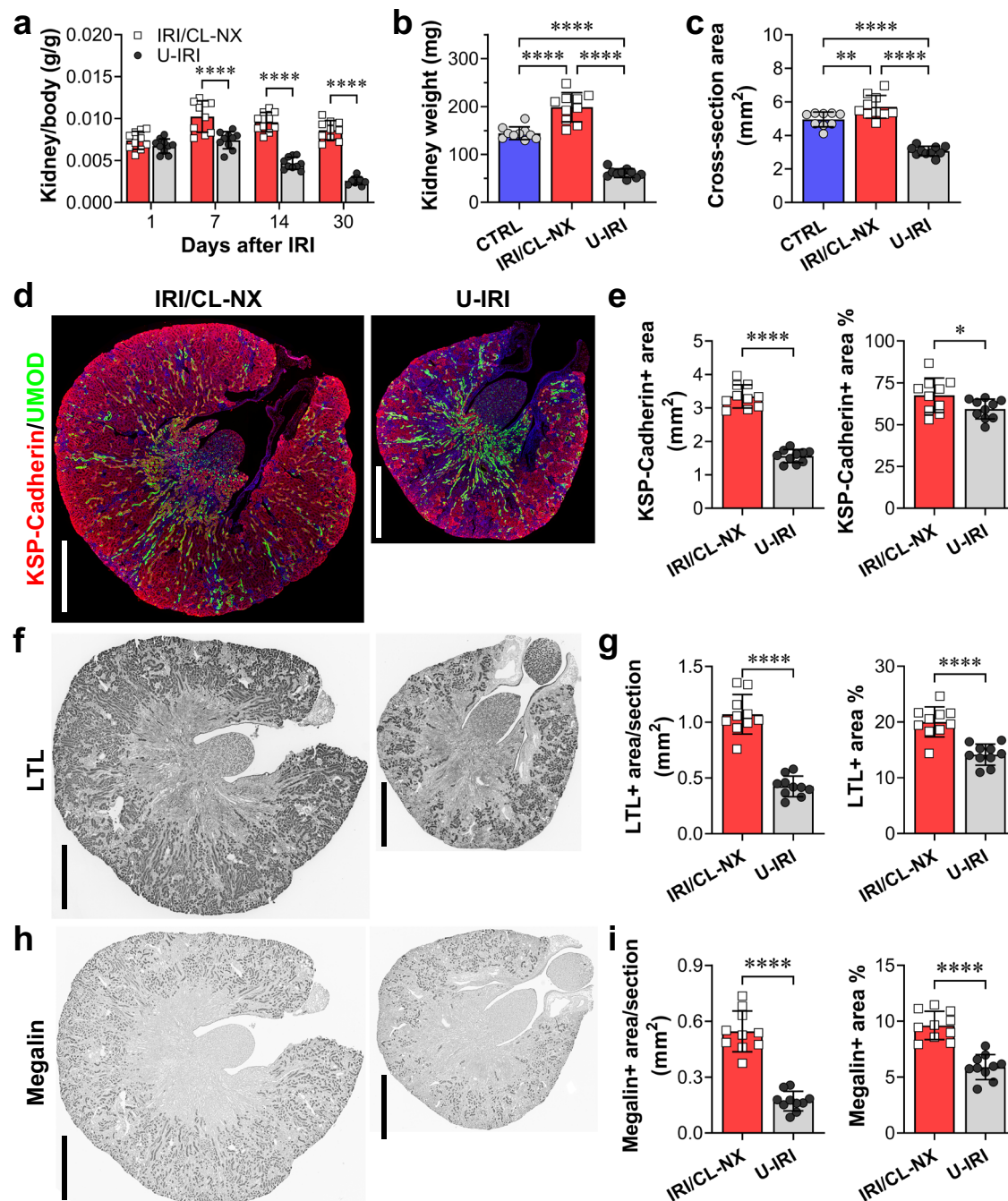


Fig. 1 | U-IRI leads to tubule atrophy. Wild-type mice were subjected to 27 min of ischemia/reperfusion injury (IRI) with contralateral nephrectomy (IRI/CL-NX) or unilateral IRI (U-IRI) and sacrificed on day 1, 7, 14, and 30 after injury. **a** Kidney-to-body weight ratios were determined on day 1, 7, 14, and 30 after injury. Data are presented as mean \pm SD. $n = 10$ kidneys/time point. $p < 0.0001$ between models and in time series (by two-way ANOVA); $****p < 0.0001$ in the indicated subgroup analyses (by Bonferroni multiple comparison). **b** Kidney weights were determined on day 30 after injury. CTRL, age-matched control. Data are presented as mean \pm SD. $n = 9$ control kidneys. $n = 10$ kidneys/model. $p < 0.0001$ by one-way ANOVA; $****p < 0.0001$ in the indicated subgroup analyses (by Tukey multiple comparison). **c** Midline kidney cross-section area was determined on day 30 after injury. CTRL, age-matched control. Data are presented as mean \pm SD. $n = 9$ control kidneys. $n = 10$ injured kidneys/model. $p < 0.0001$ by one-way ANOVA; $**p < 0.01$ ($p = 0.0075$), $****p < 0.0001$ in the indicated subgroup analyses (by Tukey multiple comparison). **d** Midline kidney sections on day 30 after IRI were co-stained with kidney-specific

(KSP)-cadherin (red), uromodulin (UMOD), and DAPI (blue). Scale bars, 1 mm. **e** KSP-cadherin-positive area as in **d** was quantified for the entire kidney section (left panel) and as a percentage of the section area (right panel). Data are presented as mean \pm SD. $n = 10$ kidneys/model. $*p < 0.05$ ($p = 0.0424$), $****p < 0.0001$ by unpaired two-tailed t -test. **f** Midline kidney sections underwent IHC staining for lotus tetragonolobus lectin (LTL, dark gray) on day 30 after IRI. Scale bars, 1 mm. **g** LTL-positive area as in **f** was quantified for the entire kidney section (left panel) and as a percentage of the section area (right panel). Data are presented as mean \pm SD. $n = 10$ kidneys/model. $****p < 0.0001$ by unpaired two-tailed t -test. **h** Midline kidney sections underwent IHC staining for megalin (dark gray) on day 30 after IRI. Scale bars, 1 mm. **i** Megalin-positive area as in **h** was quantified for the entire kidney section (left panel) and as a percentage of the section area (right panel). Data are presented as mean \pm SD. $n = 10$ kidneys/model. $****p < 0.0001$ by unpaired two-tailed t -test.

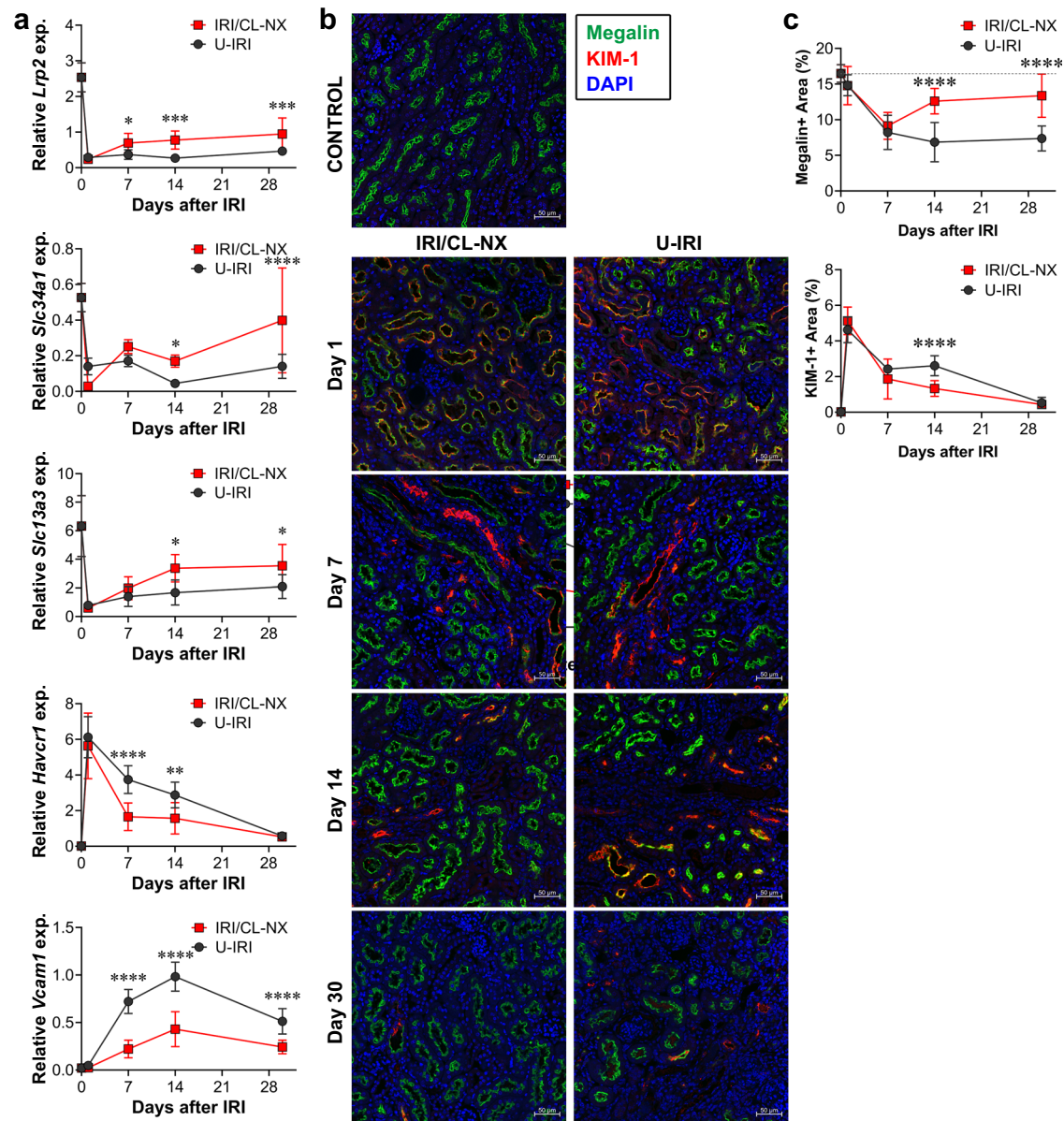


Fig. 2 | U-IRI leads to failure of tubular redifferentiation and exaggerated *Vcam1* expression. Wild-type mice were subjected to 27 min of ischemia/reperfusion injury (IRI) with contralateral nephrectomy (IRI/CL-NX) or unilateral IRI (U-IRI) and sacrificed on day 1, 7, 14, and 30 after injury. The injured kidneys and normal control kidneys (defined as day 0) were harvested. **a** Quantitative RT-PCR analysis for *Lrp2* (megalin), *Slc34a1* (sodium-dependent phosphate transporter 2A, Napi2a), *Slc13a3* (sodium-dependent dicarboxylate transporter, NaDC3), *Havcr1* (kidney injury molecule-1, Kim1), and *Vcam1* (vascular cell adhesion molecule-1) was performed on whole-kidney RNA. Data are presented as mean \pm SD. $n = 10$ kidneys/time point/model. Two-way ANOVA was summarized in Supplementary Table 1.

* $p < 0.05$, *** $p < 0.001$, **** $p < 0.0001$ at the indicated time points (by Bonferroni multiple comparison). **b** Midline kidney sections underwent IF staining for megalin (green) and KIM-1 (red) on day 0, 1, 7, 14, and 30 after IRI with representative images shown at 20 \times . Scale bars, 50 μ m. **c** Megalin+ (top) and KIM-1+ (bottom) areas as in **b** were quantified as a percentage of 6–10 randomly selected areas/kidney section. Data are presented as mean \pm SD. $n = 8$ kidneys quantified/model. Two-way ANOVA [$p < 0.0001$ (interaction, time factor, and model factor) for megalin; $p = 0.0003$ (interaction), $p < 0.0001$ (time factor), $p = 0.0228$ (model factor) for KIM-1], **** $p < 0.0001$ at the indicated time points (by Bonferroni multiple comparison).

(F4/80) and *Cd68*), dendritic cells (*Itgax*), neutrophils (*Ly6g*) and T cells (*Cd3e*, *Cd4* and *Cd8a*) significantly increased in the U-IRI model after day 7, with T cell, macrophage and dendritic cell markers remaining high through day 30 (Fig. 4a and Supplementary Fig. 5a). IHC staining for F4/80, CD11c, Ly6G, CD3 ϵ , CD4, and CD8 α on day 14 after injury confirmed that the numbers of interstitial macrophages, DCs, neutrophils, CD4+ T helper cells, and CD8+ cytotoxic T cells were significantly higher in the cortex of U-IRI kidneys as compared to contralateral and IRI/CL-NX kidneys, and all but Ly6G were higher in the outer medulla in the U-IRI model (Fig. 4b, c and Supplementary Figs. 6–11). Together, these data

demonstrate that macrophages and dendritic cells are the major cell responders in the first 7 days after IRI in both injury models, with the number of macrophages, T cells and neutrophils plateauing between 7 and 14 days in the IRI/CL-NX model whereas macrophage numbers continue increasing between days 7 and 14 in the U-IRI model accompanied by a second wave of immune activation involving recruitment of neutrophils and T cells. The macrophages present in injured kidneys after day 7 express decreasing levels of proreparative arginase 1 (*Arg1*)²⁸ with increased profibrotic gene expression predominantly in the U-IRI kidneys (Supplementary Fig. 5b–f).

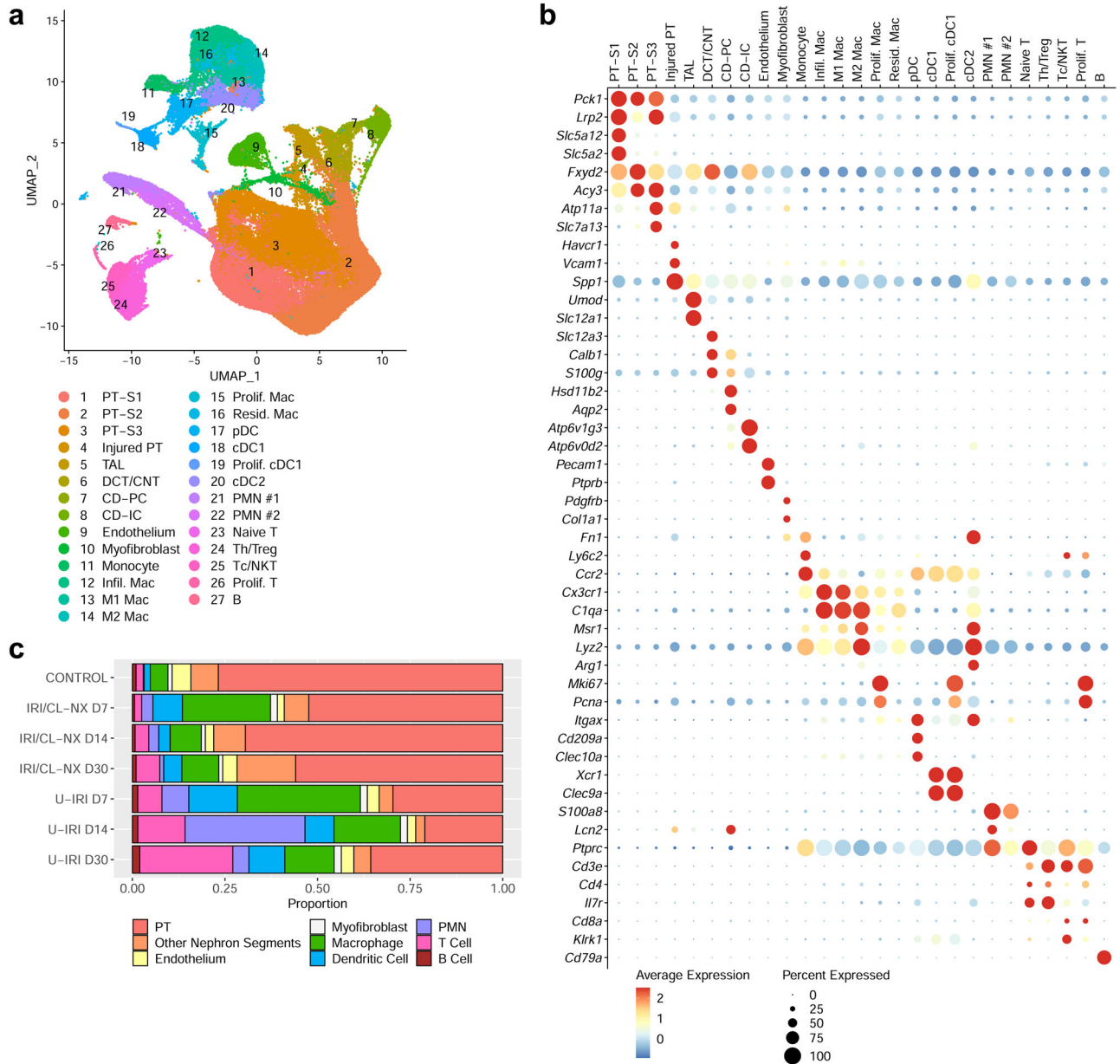


Fig. 3 | Integrated scRNA-seq analysis of differential cell type populations between IRI/CL-NX and U-IRI kidneys and control kidneys. Wild-type mice were subjected to 27 min of ischemia/reperfusion injury (IRI) with contralateral nephrectomy (IRI/CL-NX) or unilateral IRI (U-IRI) and sacrificed on day 7, 14, and 30 after injury. Injured kidneys ($n = 2$ kidneys/model/time point) and normal control kidneys ($n = 2$ kidneys) were harvested for single-cell-RNA-sequencing analysis. **a** UMAP projection of 95,343 cells from integrated kidneys. Cell clusters were identified using the composite data from all cells by kidney cell and immune cell lineage-specific marker expression as shown in **b**. PT, proximal tubule; TAL, thick

ascending limb; DCT, distal convoluted tubule; CNT, connecting tubule; CD-PC, collecting duct-principal cell; CD-IC, collecting duct-intercalated cell; Infil. Mac, infiltrating macrophage; Mac, macrophage; Prolif. Mac, proliferating macrophage; Resid. Mac, resident macrophage; pDC, plasmacytoid dendritic cell; cDC, conventional dendritic cell; PMN, polymorphonuclear neutrophil; Naive T, naïve T cell; Th/Treg, T helper/regulatory T cell; Tc/NKT, cytotoxic T/natural killer T cell; B, B cell. **c** The percentage of the cell populations is provided for each group. The number of cells in each cluster/kidney is summarized in Supplementary Table 2.

Chemokine-receptor interactions define the immune signature of the second wave of inflammation

To identify pathways mediating the second wave of immune cell recruitment following IRI, we analyzed the gene expression of homing receptors and their known chemokine ligands in the integrated single-cell dataset from both injury models. Macrophages predominantly expressed *Ccr2*, *Ccr5* and *Cx3cr1*; DCs expressed *Ccr2* and *Xcr1*; neutrophils expressed *Ccr1*, *Cxcr2*, and *Cxcr4*; and T cells expressed *Cxcr3* and *Cxcr6* (Supplementary Fig. 12). Corresponding homing chemokines for macrophages included the *Ccr2* ligands *Ccl2*, *Ccl7*, and *Ccl12* (expressed by macrophages themselves); the *Ccr5* ligands *Ccl3*, *Ccl4*

and *Ccl8* (made by macrophages and/or neutrophils); and the *Cx3cr1* ligand *Cx3cl1* (expressed at low levels by Injured PT and myofibroblasts) (Supplementary Figs. 13 and 14). Chemokines for neutrophil recruitment and activation included the *Ccr1* ligands *Ccl3*, *Ccl5*, *Ccl8* and *Ccl9* (expressed by neutrophils, $Cd8a + T$ cells, macrophages and dendritic cells, respectively); the *Cxcr2* ligand *Cxcl2* (expressed by neutrophils); and the *Cxcr4* ligand *Cxcl12* (expressed by myofibroblasts at a low level). Finally, T-cell recruitment and activation appears to predominantly depend on the *Cxcr6* ligand *Cxcl16* (expressed by macrophages) since the other potential T-cell recruitment chemokines were expressed either at low levels (*Cxcl9* and *Cxcl10*) or were not

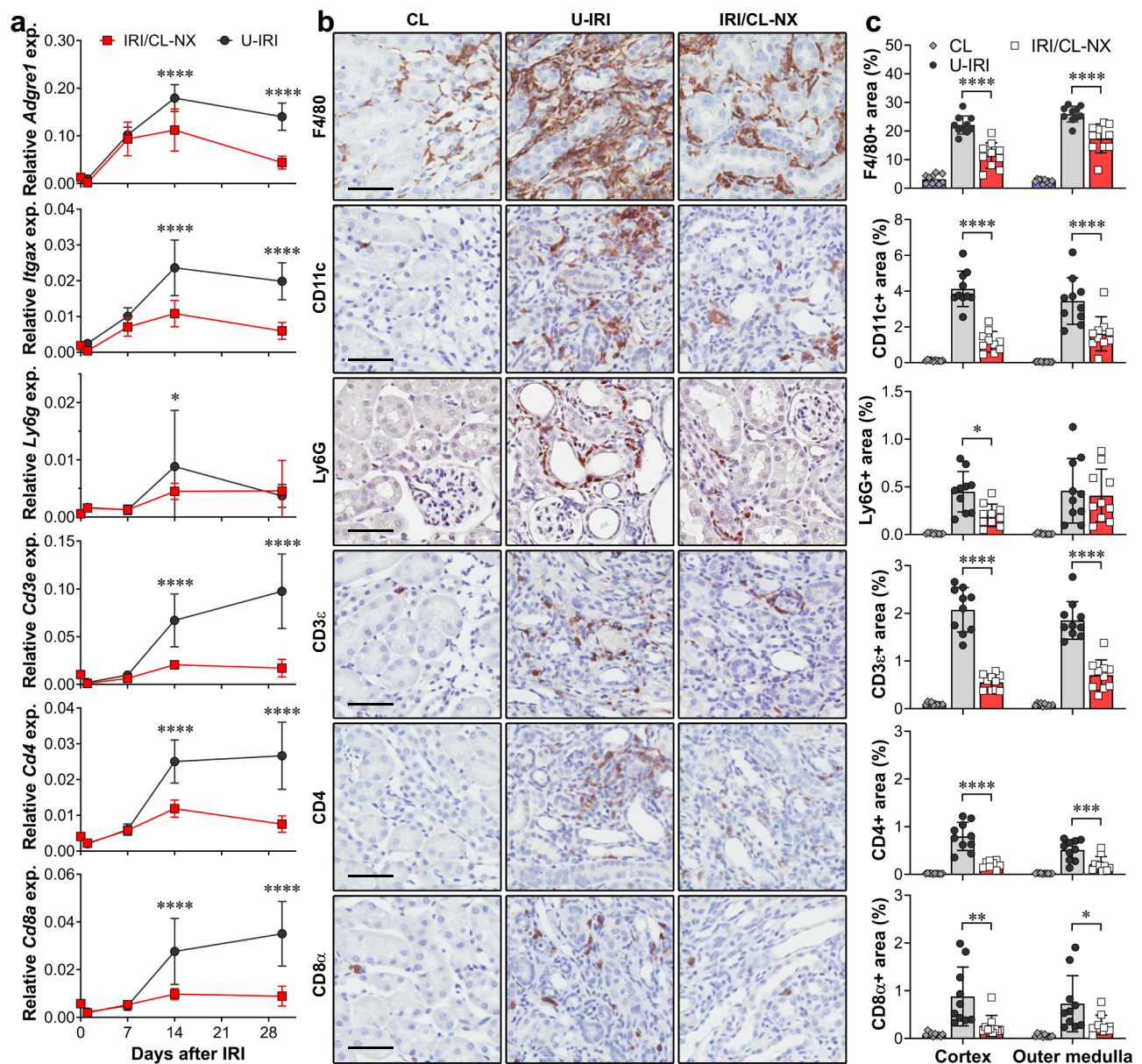


Fig. 4 | U-IRI promotes late immune cell accumulation. Wild-type mice were subjected to 27 min of ischemia/reperfusion injury (IRI) with contralateral nephrectomy (IRI/CL-NX) or unilateral IRI (U-IRI) and sacrificed on day 1, 7, 14, and 30 after injury. The injured kidneys and normal control kidneys (defined as day 0) were analyzed. **a** Quantitative RT-PCR analysis for *Adgre1* (F4/80), *Itgax*, *Ly6g*, *Cd3e*, *Cd4*, and *Cd8a* was performed on whole-kidney RNA. Data are presented as mean \pm SD. $n = 10$ kidneys/time point/model. Two-way ANOVA is summarized in Supplementary Table 1. * $p < 0.05$ ($p = 0.0449$), **** $p < 0.0001$ at the indicated time

points (by Bonferroni multiple comparison). **b** Contralateral (CL), U-IRI and IRI/CL-NX kidney sections on day 14 after IRI were immunostained with F4/80, CD11c, Ly6G, CD3ε, CD4, and CD8α. Images that are representative of those taken from 10 kidneys/model are shown at 40x magnification. Scale bars, 50 μm. **c** F4/80-, CD11c-, Ly6G-, CD3ε-, CD4-, and CD8α-positive areas as in **b** were quantified. Data were presented as mean \pm SD. $n = 10$ kidneys/group. Two-way ANOVA is summarized in Supplementary Table 3. * $p < 0.05$, ** $p < 0.01$, **** $p < 0.0001$ in the indicated subgroup analyses by Tukey multiple comparison.

detected (*Cxcl11*) (Supplementary Figs. 13 and 14). Together, the data suggests that infiltrating, M1, and M2 macrophages are the predominant cells to express immune-recruiting chemokines in the injured kidneys.

To better understand how macrophages signal in response to unresolved injury, we identified the differentially expressed genes (DEG) of infiltrating, M1, and M2 macrophages between the U-IRI and IRI/CL-NX kidneys. On day 14, we found a set of chemokines including *Ccl2*, *Ccl7*, *Ccl8*, and *Ccl12*, that were significantly upregulated in all three macrophage populations from the U-IRI kidneys as compared to the IRI/CL-NX kidneys (Fig. 5a–d). The upregulation of these chemokines by day 14 in U-IRI kidneys correlates with the second wave of immune cells observed on days 14 and 30 in this model (Fig. 4a).

Quantitative PCR for the macrophage receptor *Ccr2* and its activating chemokines *Ccl12*, *Ccl7* and *Ccl2*²⁹; the neutrophil receptor *Ccr1* and its activating chemokine *Ccl8*; and the T-cell receptor *Cxcr6* and its activating chemokine *Cxcl16* from whole-kidney mRNA confirmed the significant increase of these ligand-receptor pairs between days 14 and 30 in the U-IRI injury model (Fig. 5e and Supplementary Fig. 15).

To identify which of these ligand-receptor interactions resulted in functional immune cell responses, we utilized the NicheNet ligand-receptor-target algorithm developed by Saeys and colleagues^{30,31}. Since the chemokines were predominantly expressed by macrophages at 14 days (Supplemental Fig. 13), we focused on immune cell-secreted ligands. This analysis revealed extensive chemokine-receptor interactions between infiltrating, M1, and M2 macrophage-

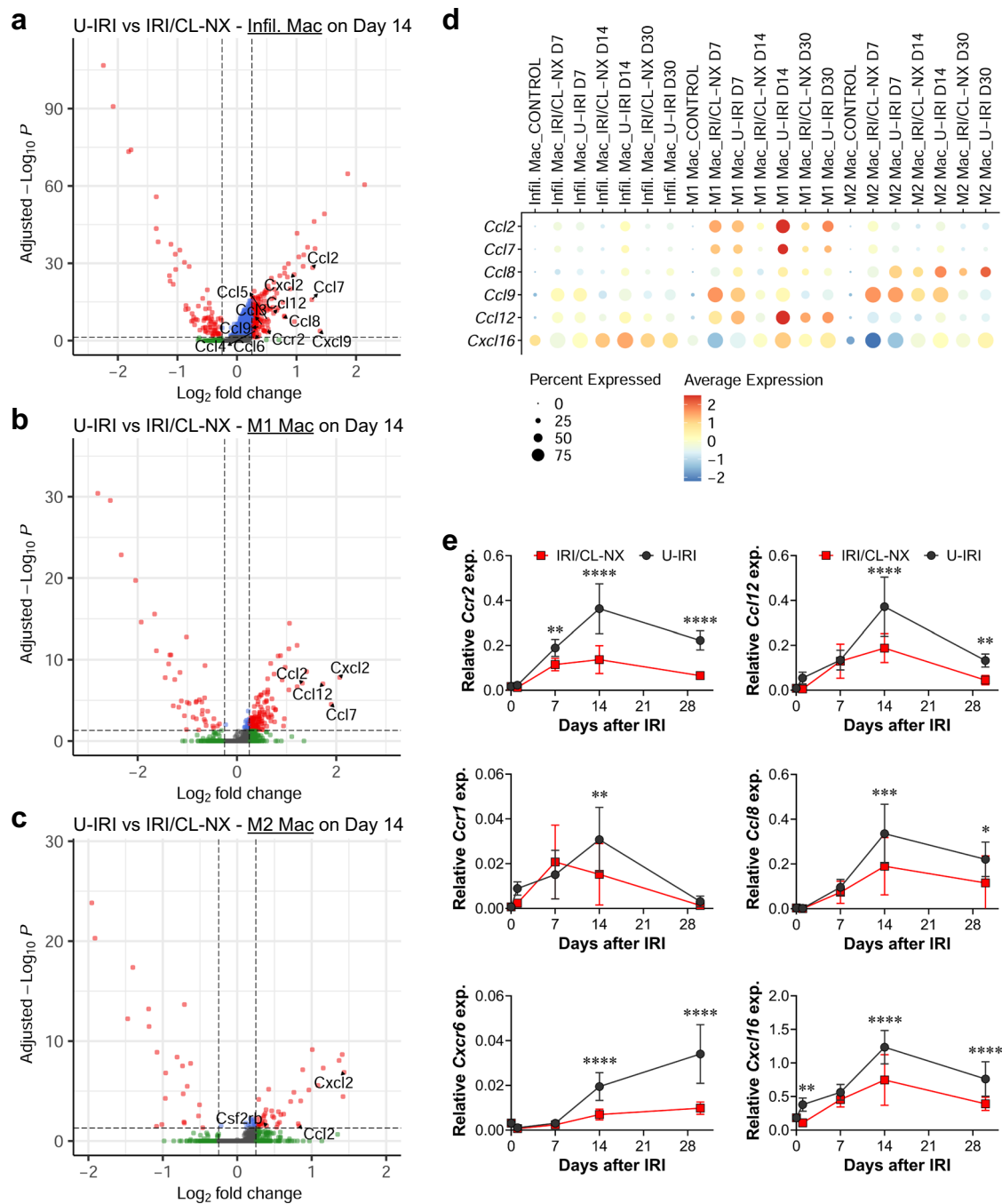


Fig. 5 | U-IRI promotes increased chemokine expression 2 weeks after IRI. Wild-type mice were subjected to 27 min of ischemia/reperfusion injury (IRI) with contralateral nephrectomy (IRI/CL-NX) or unilateral IRI (U-IRI) and sacrificed on day 7, 14 and 30 after injury. Injured kidneys and normal control kidneys were harvested for single-cell-RNA-sequencing analysis as shown in Fig. 3. **a–c** Volcano plots demonstrating differential gene expression in infiltrating macrophages (Infil. Mac, **a**); proinflammatory macrophages (M1 Mac, **b**); and alternatively activated macrophage (M2 Mac, **c**) on day 14 after U-IRI compared to IRI/CL-NX. **d** The

distribution and relative expression of chemokines are visualized in the dot plot. D7, Day 7; D14, Day 14; D30, Day 30. **e** Quantitative RT-PCR analysis for the indicated chemokines and chemokine receptors was performed on whole-kidney RNA harvested on day 0, 1, 7, 14, and 30 after injury. Data are presented as mean \pm SD. $n=10$ kidneys/time point/model. Two-way ANOVA is summarized in Supplementary Table 1. * $p < 0.05$, ** $p < 0.01$, *** $p < 0.001$, **** $p < 0.0001$ at the indicated time points (by Bonferroni multiple comparison).

secreted ligands and their receptors on neutrophils (*Ccr1*, *Cxcr2*, and *Cxcr4*), $Cd4^+$ Th/Treg, and $Cd8a^+$ Tc/NKT (*Ccr2*, *Ccr5*, *Cxcr3*, and *Cxcr6*) (Fig. 6a, b and Supplementary Figs. 16 and 17). For example, *Ccl3*, *Ccl4*, and *Ccl8* that were significantly upregulated in M1 and M2 macrophages on day 14 after U-IRI are predicted to interact with *Ccr1*-expressing cells such as PMN cluster #1. As a result, the pathways involved in leukocyte (neutrophils, monocytes, and lymphocytes) chemotaxis were significantly enriched in the infiltrating and M1

macrophages (Fig. 6c). The functional role of these macrophage-secreted chemokines in recruiting the second wave of T cells and PMNs was supported by numerous examples of both $CD3\epsilon^+$ T cells and $Ly6G^+$ PMNs found adjacent to $F4/80^+$ macrophages in kidneys 14 days after U-IRI (Fig. 6d). Taken together, these data show that macrophages that persist beyond day 7 in U-IRI kidneys are selectively activated to express high levels of chemokines that are predicted to promote a second wave of inflammatory neutrophil and

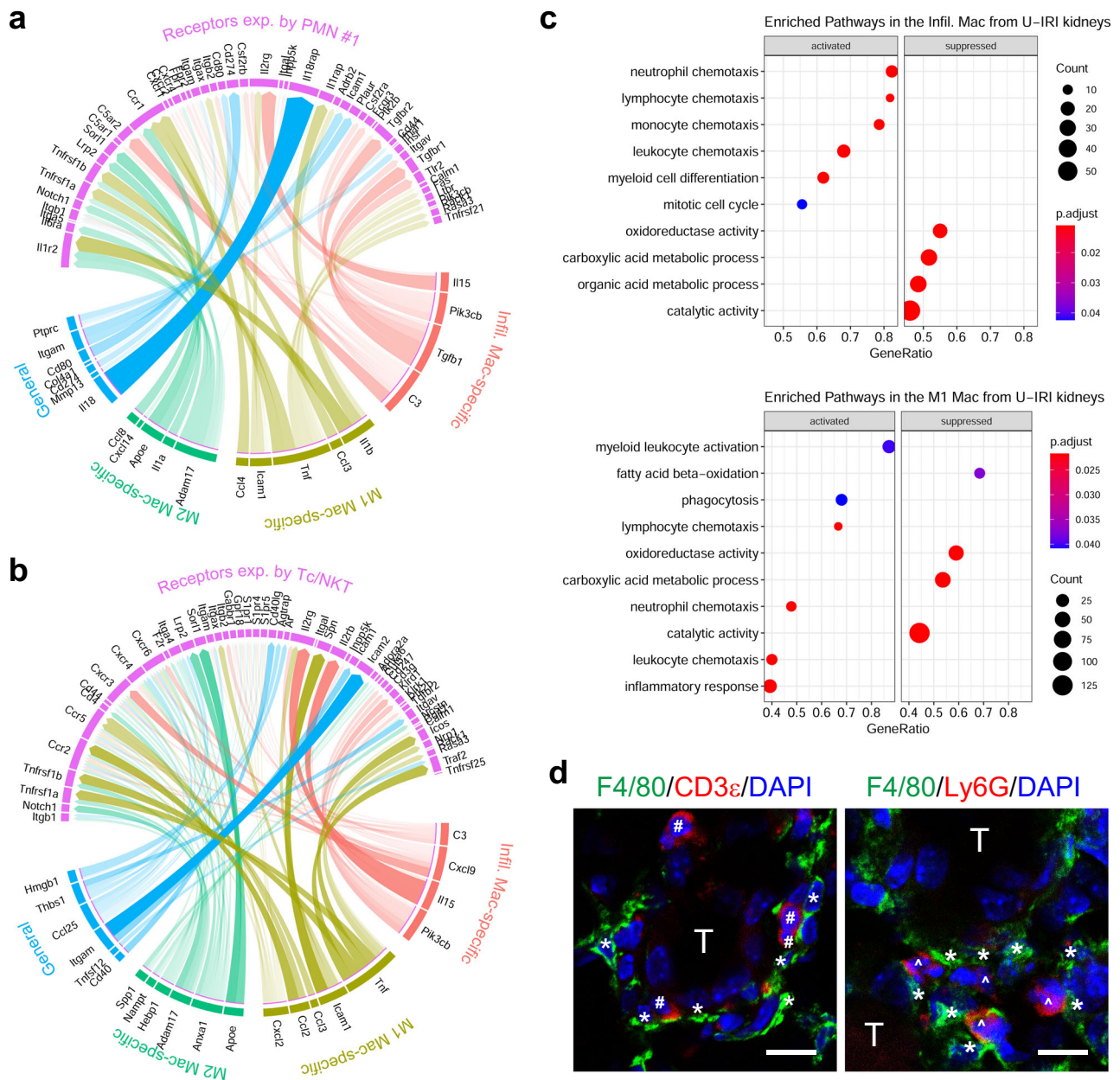


Fig. 6 | U-IRI promotes a second wave of immune cell recruitment. Wild-type mice were subjected to 27 min of ischemia/reperfusion injury (IRI) with contralateral nephrectomy (IRI/CL-NX) or unilateral IRI (U-IRI) and sacrificed on day 7, 14, and 30 after injury. Injured kidneys and normal control kidneys were harvested for single-cell-RNA-sequencing analysis as shown in Fig. 3. **a, b** Genes that were differentially expressed on day 14 after injury by the infiltrating (Infil.), M1, M2 macrophages (Mac), and in any combination (General) in U-IRI kidneys as compared to IRI/CL-NX kidneys were linked to their corresponding receptors based on

the potential target genes (as shown in Supplementary Fig. 16) expressed by polymorphonuclear neutrophil cluster #1 (PMN #1) (**a**) and cytotoxic T/natural killer T (Tc/NKT) cells (**b**) and visualized by a chord diagram. **c** The top relevant enriched gene ontology (GO) terms for infiltrating (top panel) and M1 (lower panel) macrophages are visualized in the dot plots. **d** Representative images of immunofluorescence (IF) staining for F4/80 (green), CD3ε (red on the left panel), and Ly6G (red on the right panel) using cryosections from three kidneys 14 days after U-IRI. T, tubules; *, macrophages; #, T cells; ^, PMNs. Scale bars: 10 μm.

T-cell recruitment, resulting in a local nidus for extensive inter- and intra-immune cell cross-talk^{32,33}.

Late immune activation promotes tubule oxidative stress and secondary injury

To understand the impact of this second wave of immune activation on tubule injury and atrophy, we determined the DEG in PMNs, Tc/NKT, and Th/Tregs between the U-IRI and IRI/CL-NX kidneys. On day 14, we found that PMNs in the U-IRI kidney significantly upregulated inflammatory gene expression including *Il1b*, *Il1f9*, *Tnf*, *Tnfaip3*, *Ifitm1*, and *Lcn2* (Fig. 7a, b). Cd8+ Tc/NKT cells in the U-IRI kidney expressed

significantly higher levels of T-cell activation genes such as *Tyrobp*, *Klre1*, *Serpinb9*, *Ripor2*, *Fasl*, *Xbp1*, and *Zfp36l2* (Fig. 7c). Cd4+ Th/Treg cells in the U-IRI kidneys also showed increased expression of T-cell activation genes such as *Fyn*, *Gpr183*, *Laptm5*, *Lax1*, *Lfng*, *Itk*, *Trp53*, and *Zfp36l1* (Supplemental Fig. 18a). The upregulation of these genes is predicted to activate pathways involved in production of interleukin 1, 6, and 12, interferon γ, nitric oxide, and superoxide anion in PMNs (Fig. 7d, e); cell killing and regulation of apoptosis in the Tc/NKT cells (Fig. 7f); and T-cell activation and antigen recognition in the Th/Treg cells (Supplemental Fig. 18a, c) on day 14 after U-IRI. Quantitative PCR analysis confirmed that the mRNA expression levels of *Il1b*, *Tnf*, *Fasl*,

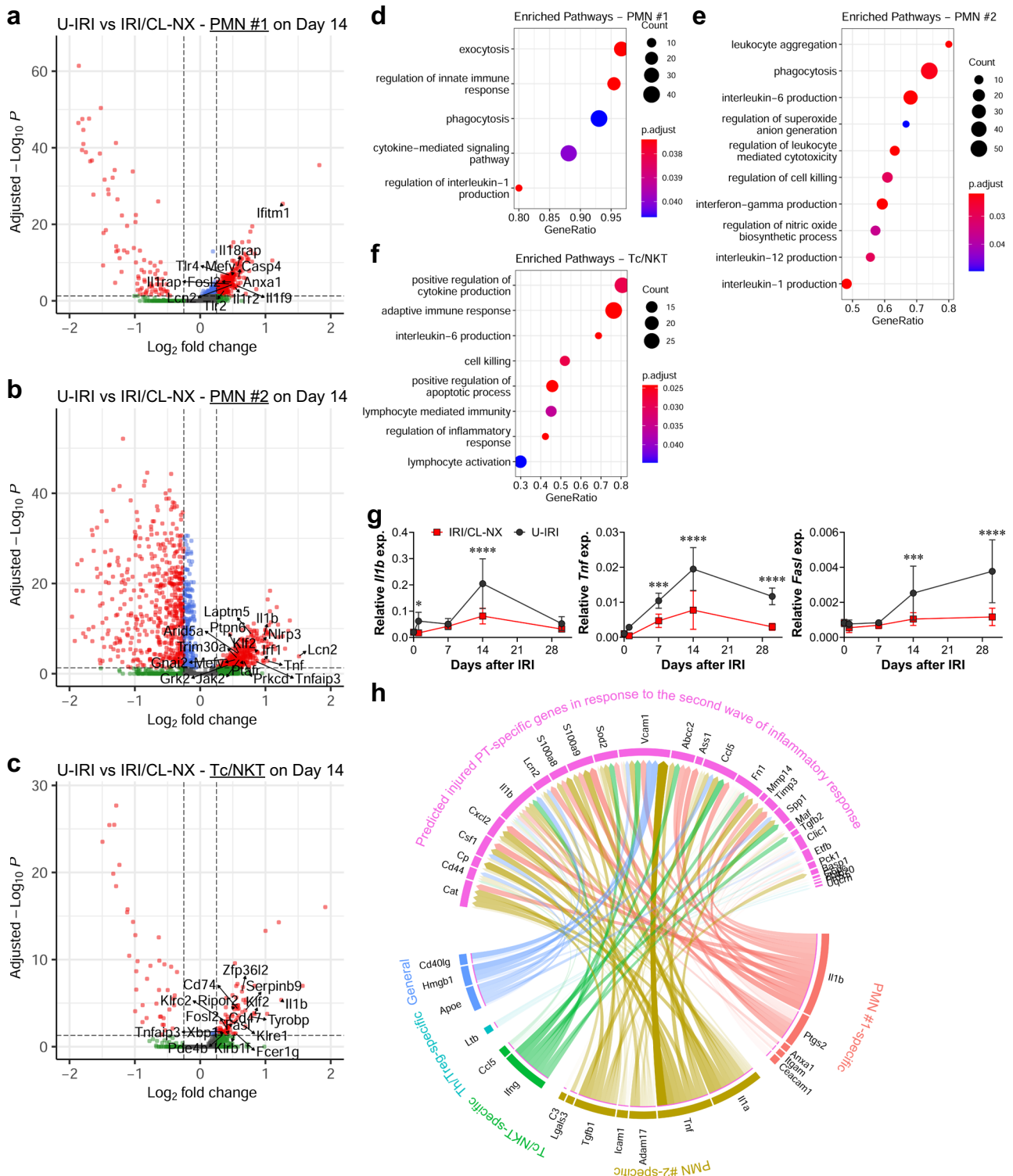


Fig. 7 | U-IRI promotes late PMN- and T- cell-mediated inflammation. Wild-type mice were subjected to 27 min of ischemia/reperfusion injury (IRI) with contralateral nephrectomy (IRI/CL-NX) or unilateral IRI (U-IRI) and sacrificed on day 7, 14, and 30 after injury. Injured kidneys and normal control kidneys were harvested for single-cell-RNA-sequencing analysis as shown in Fig. 3. **a–c** Volcano plots demonstrating differential gene expression in U-IRI compared to IRI/CL-NX derived polymorphonuclear neutrophil cluster #1 (PMN #1) (**a**), PMN cluster #2 (**b**), and Cd8a+ cytotoxic T/natural killer T (Tc/NKT) cells (**c**) on day 14 after injury. **d–f** Based on differentially expressed genes (DEG) between U-IRI and IRI/CL-NX kidneys on day 14 after injury, the top relevant enriched gene ontology (GO) terms for PMN

cluster #1 (**d**), PMN cluster #2 (**e**), and Cd8a+ Tc/NKT cells (**f**) in the U-IRI kidneys are visualized in the dot plots. **g** Quantitative RT-PCR analysis for indicated genes was performed on whole-kidney RNA harvested on day 0, 1, 7, 14, and 30 after injury. Data are presented as mean ± SD. *n* = 10 kidneys/time point/model. Two-way ANOVA is summarized in Supplementary Table 1. **p* < 0.05, ****p* < 0.001, *****p* < 0.0001 at the indicated time points (by Bonferroni multiple comparison). **h** Based on DEG between U-IRI and IRI/CL-NX kidneys on day 14 after injury, the potential ligands expressed by the PMNs, Cd8a+ Tc/NKT, and Cd4+ T helper/regulatory T (Th/Treg) cells were linked to their corresponding potential target genes for the injured proximal tubule (PT) cells and visualized by a chord diagram.

Ltb, and *Cd40lg* were increased to a greater degree 14 days after U-IRI injury as compared to those in the IRI/CL-NX kidneys (Fig. 7g and Supplemental Fig. 18b), consistent with the increase in neutrophil and T-cell number seen during the second wave of immune activation (Supplementary Tables 4 and 5). Ligand-receptor-target analyses reveals that PMNs, Tc/NKT, and Th/Treg are projected to induce PT cells to increase expression of several genes including *Vcam1*, *Spp1*, *Csf1*, and *Cp* (ferroxidase) that have been previously implicated as injury markers (Fig. 7h and Supplementary Figs. 19–21).

To define the tubular response to the second wave of immune recruitment and activation, we analyzed the DEG of PT cells between the U-IRI and IRI/CL-NX kidneys. On day 14, we found that proximal tubule cells from U-IRI kidneys expressed minimal levels of the classic acute injury marker *Havcr1* (*Kim1*), but significantly higher levels of distinct injury markers including *Vcam1*, *Csf1*, and *Spp1* (Fig. 8a–c and Supplementary Fig. 22a, b). In addition, multiple major histocompatibility complex (MHC) class II genes (*H2-Aa*, *H2-Ab1*, *H2-Eb1*, and *Cd74*) and class I genes (*H2-D1* and *H2-K1*) were upregulated in U-IRI tubular cells, while anti-oxidative stress genes (*Gpx1*, *Gpx3*, *Gpx4*, *Gsta2*, *Gstm1*, *Gstp1*, *Gatm*, and *Iscu*), as well as the PT differentiation marker (*Lrp2*) were downregulated (Fig. 8a, b and Supplementary Fig. 22a, b). This shift of gene expression by tubule cells from anti-oxidative stress genes induced following IRI/CL-NX to expression of MHC genes and non-canonical injury markers after U-IRI was observed from day 7 through day 30 and was recapitulated to a lesser degree in most nephron segments (PT, TAL, DCT/CNT, and CD; Fig. 8c). The increase of MHC class I expression is associated with the increase of *Vcam1* expression in the injured PT and *Lcn2* expression in the CD-PC cells in the U-IRI kidneys (Fig. 8c). Consistent with the single-cell data, quantitative PCR analysis confirmed that mRNA expression levels of *H2-Aa*, *H2-Ab1*, and *Cd74* were markedly upregulated in U-IRI kidneys on days 14 and 30 after injury (Fig. 8d and Supplementary Fig. 22c). The expression kinetics of *H2-Aa*, *H2-Ab1*, and *Cd74* highly correlated with the expression of T-cell markers *Cd3e*, *Cd4*, and *Cd8a* as well as *Tnf* and *Ltb* (Supplementary Table 6). Taken together, the second wave immune response correlated with increased antigen presentation, T-cell activation, and T-cell- and PMN-mediated injury in the renal tubules after U-IRI that is distinct from the injury profile seen in tubules following acute ischemic injury (Fig. 8e).

Dual depletion of T cells and neutrophils attenuates kidney atrophy and loss of nephrons

To understand whether the second wave of inflammatory T cells and neutrophils promotes kidney tubule atrophy, we depleted either neutrophils, T cells, or both beginning on day 5 following U-IRI and analyzed the phenotype of the injured kidney on day 30. We found that depletion of neutrophils and T cells together in the U-IRI model of injury (Fig. 9a–c and Supplementary Figs. 23 and 24), but not either cell type individually (Supplementary Figs. 25 and 26), improved kidney-to-body weight ratio by 20% following U-IRI (Fig. 9d). Quantitative analysis of LTL staining revealed an 80% increase in the absolute area of proximal tubule brush border following dual T-cell and neutrophil depletion, reflecting a 50% increase in the percent of the total cross-sectional area comprised of PT brush border (Fig. 9e, f). Quantitative PCR analysis confirmed that the mRNA expression levels of differentiated proximal tubular transporters *Lrp2* and *Scl34a1* increased 1.5- and 1.7-fold, respectively, following depletion of both T cells and neutrophils in the U-IRI kidneys (Fig. 9g). Together, these results suggest that the second wave of activated T cells and neutrophils promotes loss of tubule cell differentiation and reduced nephron mass following U-IRI.

Accumulation of T cells and neutrophils is negatively associated with GFR recovery in patients with AKI

Our animal model findings prompted us to investigate the relevance of T-cell and neutrophil accumulation for recovery of kidney function in

patients with AKI. To assess this, ten kidney biopsies from patients with acute kidney injury (AKI), an estimated GFR (eGFR) >60 mL/min/1.73m² prior to AKI episode, and no history or pathologic indication of glomerulonephritis (GN), diabetic kidney disease (DKD), or acute interstitial nephritis (AIN) were selected from the Yale kidney biopsy biorepository (Supplementary Tables 7 and 8)^{34,35}. For these patients, eGFR declined by an average of 61 (36, 71) mL/min at the time of AKI from their pre-AKI level with a spectrum from partial to full eGFR recovery 6 months after AKI (Fig. 10a and Supplementary Tables 7 and 8). We quantified the number of T cells and neutrophils in sections from each of these kidney biopsies, and compared to those seen in kidney biopsies from healthy living kidney donors³⁶. As expected, very few T cells or neutrophils were found in kidneys from living donors, whereas T cells and neutrophils were easily detected in the kidney interstitium of some patients at the time of biopsy for AKI (Fig. 10b). Nonparametric Spearman correlation analysis of the number of T cells or neutrophils (quantified as a percentage of total cells identified in the cortex) with either the absolute or relative increase in eGFR at 6 months after AKI revealed a strong negative correlation between inflammatory cell number and eGFR recovery following AKI (Fig. 10c, d).

Discussion

Kidney injury has been extensively investigated using mouse models of either bilateral IRI or IRI/CL-NX to develop our current mechanistic understanding of tubule injury and repair including mechanisms of cell death, the innate immune response to injury, proliferation of surviving tubular cells to replace those that are lost, clearance of casts and restoration of GFR^{37–40}. Recently, our group and others have shown that performing U-IRI with the contralateral kidney intact leads to a different outcome in which fibrosis and kidney atrophy predominate rather than tubule repair and restoration of function^{7,20,21,37}.

In this study, we show that the initial macrophage, DC, neutrophil and T-cell response to ischemia/reperfusion injury is similar during the first 7 days after injury in the two models. However, after 7 days the responses markedly diverge with a surge in T cells and neutrophils observed in the U-IRI kidneys as compared to IRI/CL-NX kidneys. The divergence becomes detectable on day 7 with continued *Kim1* expression by the proximal tubule and de novo upregulation of *Vcam1*, and ends with extensive kidney atrophy by day 30. As previously reported by our group and others, the decreased kidney size following U-IRI is accompanied by excessive macrophage persistence and a transition to a *Pdgfb*+ and *Tgfb1*+ profibrotic expression profile^{20,21}. However, quantitative analysis of the remaining tubule area relative to total kidney area suggests that the major phenotypic change underlying kidney atrophy after U-IRI is tubule loss rather than increased fibrosis (Fig. 1). In fact, the transition of macrophages to a profibrotic phenotype was seen in both models of IRI (Supplementary Fig. 5b–f), consistent with evidence that even “reparative” models of kidney injury such as IRI/CL-NX or bilateral IRI lead to increased kidney fibrosis^{29,41}.

Similar to the results of Liu and colleagues who studied the slowly progressive kidney atrophy and fibrosis seen following bilateral IRI⁴¹, we find that the accelerated renal atrophy following U-IRI correlates with sustained tubular injury and inflammatory cell activation. By performing single-cell sequencing and cell-cell ligand-receptor-target interaction analyses, we now demonstrate that this delayed increase in inflammation in the U-IRI kidneys correlates with the unique chemokine (*Ccl2*, *Ccl7*, *Ccl8*, *Ccl12*, and *Cxcl16*) expression by macrophages, that in turn can recruit more macrophages²¹, as well as a second wave of infiltrating proinflammatory neutrophils and T cells between 7 and 30 days after injury.

Initial neutrophil recruitment and transmigration peaks at ~24 h after IRI and promotes reactive oxygen species (ROS) production, activation of resident mononuclear phagocytes, and differentiation of

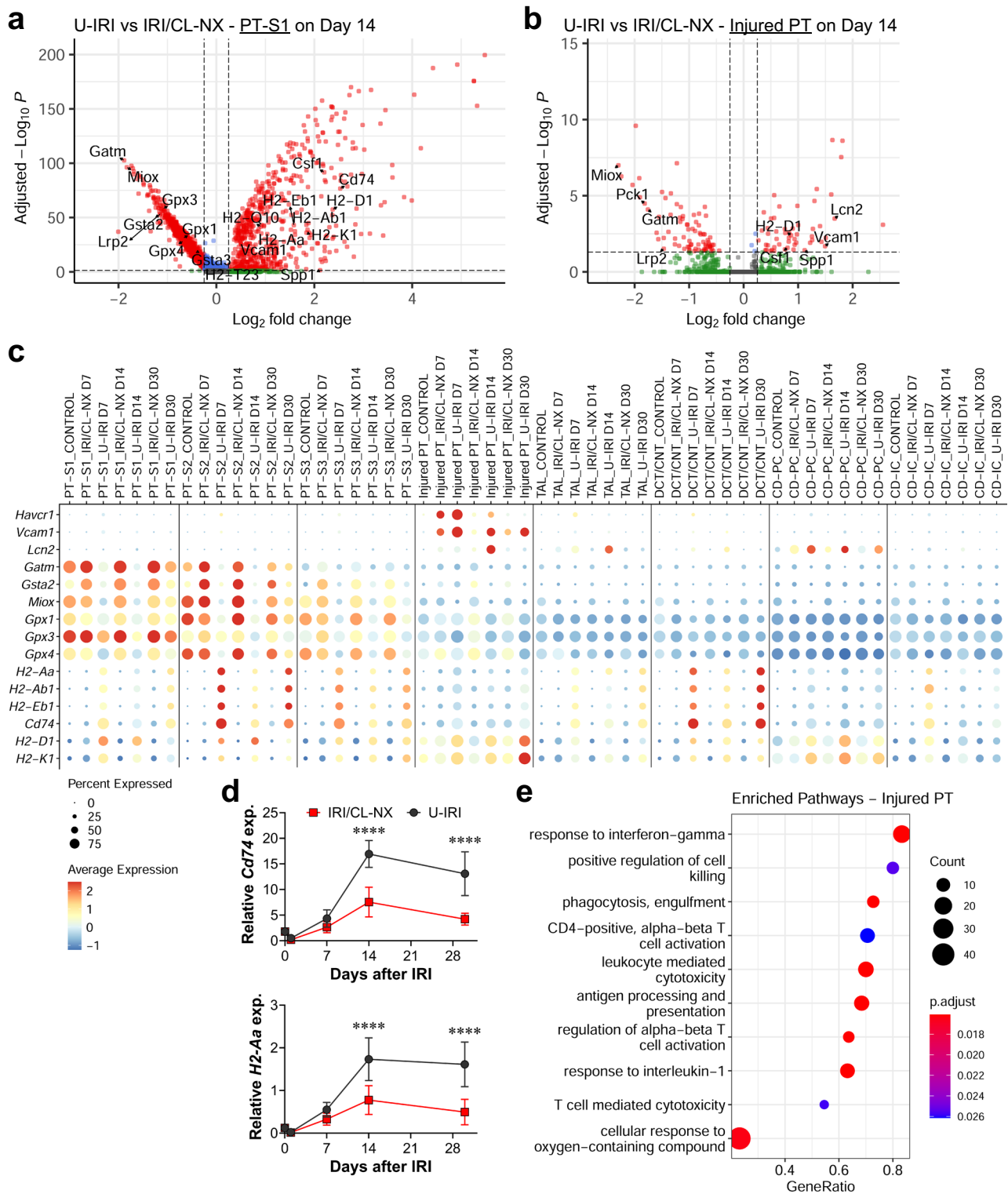


Fig. 8 | Identifying the injury signature of inflammation-induced tubular stress. Wild-type mice were subjected to 27 min of ischemia/reperfusion injury (IRI) with contralateral nephrectomy (IRI/CL-NX) or unilateral IRI (U-IRI) and sacrificed on day 7, 14, and 30 after injury. Injured kidneys and normal control kidneys were harvested for single-cell-RNA-sequencing analysis as shown in Fig. 3. **a, b** Volcano plots demonstrating the differential gene expression in cells from segment 1 of the proximal tubule (PT-S1, **a**) and injured PT (**b**) 14 days after U-IRI compared to IRI/CL-NX. **c** The distribution and relative expression of the injury markers (*Havcr1*, *Vcam1*, and *Lcn2*), anti-oxidative stress and detoxification genes (*Gatm*, *Gsta2*, *Miox*, *Gpx1*, *Gpx3*, and *Gpx4*), and the major histocompatibility complex class II (*H2-Aa*, *H2-Ab1*,

H2-Eb1, and *Cd74*) and class I (*H2-D1* and *H2-K1*) are visualized in a dot plot. **d** Quantitative RT-PCR analysis for indicated genes was performed on whole-kidney RNA harvested on day 0, 1, 7, 14, and 30 after injury. Data are presented as mean ± SD. *n* = 10 kidneys/time point/model. Two-way ANOVA is summarized in Supplementary Table 1. *****p* < 0.0001 at the indicated time points (by Bonferroni multiple comparison). **e** Based on differentially expressed genes (DEG) between U-IRI and IRI/CL-NX kidneys on day 14 after injury, the top relevant enriched gene ontology (GO) terms for injured proximal tubule (PT) in the U-IRI kidneys are visualized in the dot plots.

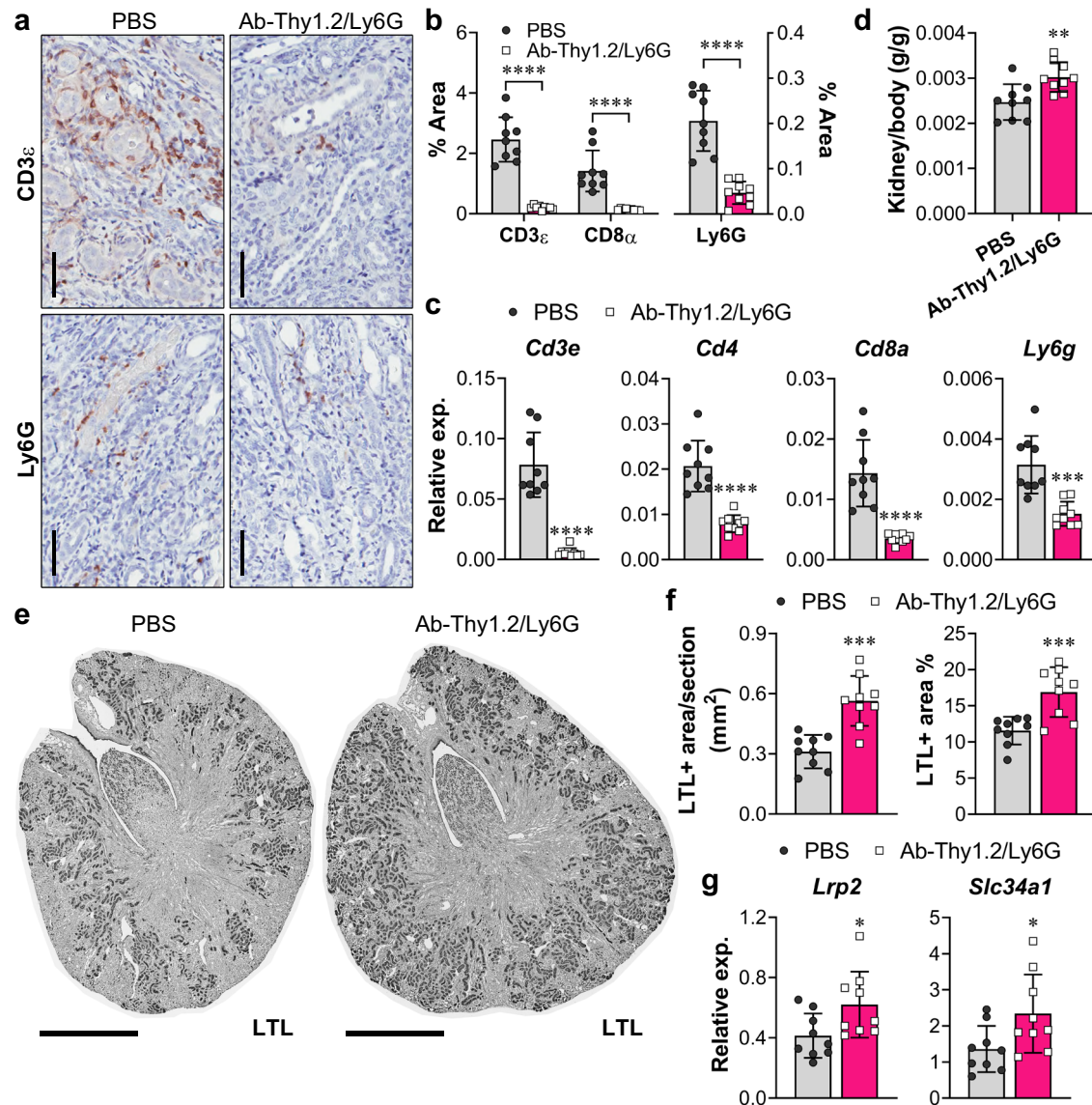


Fig. 9 | Dual depletion of T cells and neutrophils attenuates kidney tubule atrophy. WT mice were treated as described in Methods with either PBS or a combination of antibodies (Ab)-against Thy1.2 and Ly6G beginning 5 days after unilateral ischemia/reperfusion injury (U-IRI) and sacrificed on day 30. **a** The IRI kidney sections were immunostained with CD3 ϵ and Ly6G. Nine kidneys/group were sectioned and stained, and representative images are shown. Scale bars, 25 μ m. **b** CD3 ϵ -, CD8 α -, and Ly6G-positive areas were quantified using Image J. Data are presented as mean \pm SD. $n = 9$ kidney sections/group. **** $p < 0.0001$ by unpaired two-tailed t -test. **c** Quantitative RT-PCR analysis for *Cd3e*, *Cd4*, *Cd8a*, and *Ly6g* was performed on whole-kidney RNA on day 30 after U-IRI \pm dual T-cell/neutrophil depletion. Data are presented as mean \pm SD. $n = 9$ kidneys/group. **** $p < 0.001$, **** $p < 0.0001$ by unpaired two-tailed t -test. **d** Kidney-to-body weight

ratios on day 30 following U-IRI \pm dual T-cell/neutrophil depletion. Data are presented as mean \pm SD. $n = 9$ kidneys/group. ** $p < 0.01$ by unpaired two-tailed t -test. **e** Kidney sections from day 30 after U-IRI \pm dual T-cell/neutrophil depletion were immunostained with lotus tetragonolobus lectin (LTL, dark gray). Nine kidneys were sectioned and stained and representative images are shown. Scale bars, 1 mm. **f** LTL-positive area was quantified from the entire section (left panel) and as a percentage of the section (right panel). Data are presented as mean \pm SD. $n = 9$ kidneys/group. *** $p < 0.001$ by unpaired two-tailed t -test. **g** Quantitative RT-PCR analysis for *Lrp2* and *Slc34a1* was performed on whole-kidney RNA from U-IRI mice \pm dual T-cell/neutrophil depletion. Data are presented as mean \pm SD. $n = 9$ kidneys/group. * $p < 0.05$ by unpaired two-tailed t -test.

recruited monocytes into proinflammatory macrophages, all of which contribute to the early components of reperfusion injury⁶. In models of injury where repair pathways predominate, CD169⁺ macrophages limit subsequent neutrophil infiltration in the kidney by down-regulating intercellular adhesion molecule-1 (ICAM-1) expression on vascular endothelial cells⁴², and neutrophil numbers in the interstitium dramatically decrease after day 3, corresponding to the period when proreparative macrophages become prominent. In contrast, intrarenal T cells are not typically seen in large numbers in the first week after IRI, but have been identified in the late stages of IRI where they can promote upregulation of proinflammatory cytokine expression including

Il1b, *Il6*, *Tnf*, and *Ifng*^{43–45}. We now show that in a model where atrophy predominates, this late neutrophil and T-cell infiltrate correlates with sustained tubular cell dedifferentiation and the increased expression of multiple homing chemokines by macrophages as well as the infiltrating T cells and neutrophils themselves.

Infiltrating T cells can be activated through antigen-independent mechanisms by inflammatory cytokines and reactive oxygen intermediates as well as through interaction with antigen-presenting cells (APCs). Our results illustrate that in response to the late cell stress induced by inflammatory cytokines, proximal tubular epithelial cells in U-IRI kidneys upregulated MHC class II (*H2-Aa*, *H2-Ab1*, *H2-Eb1*, and

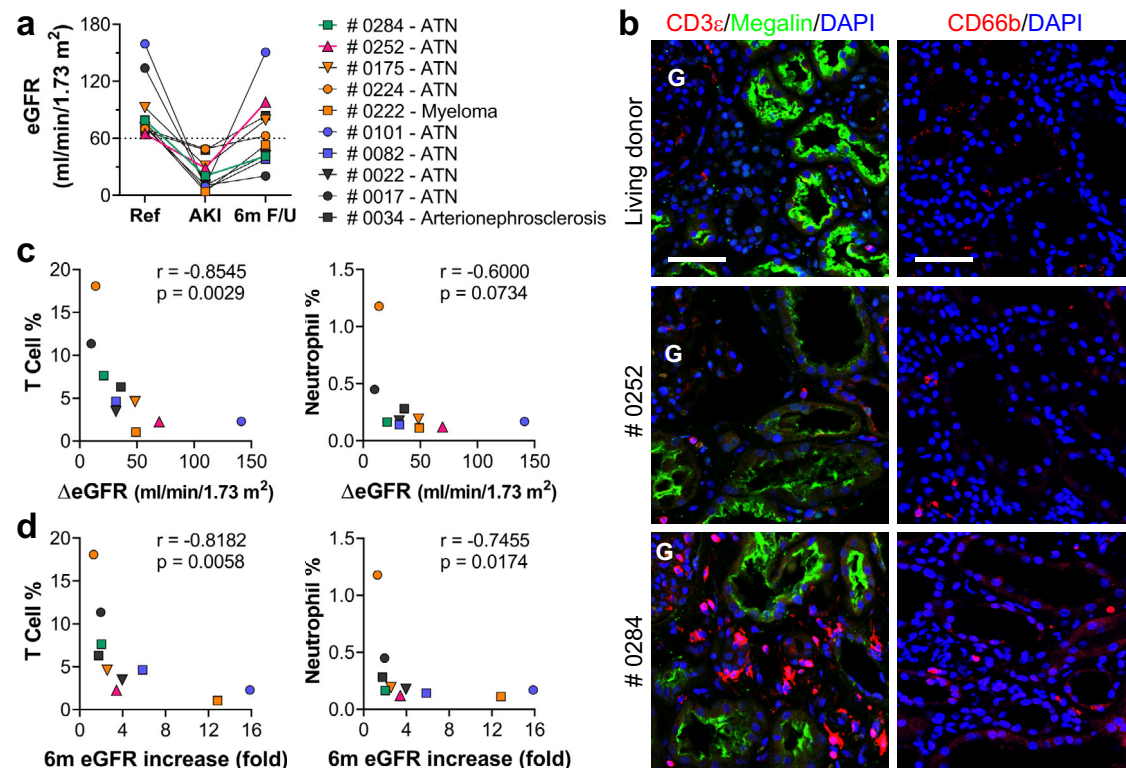


Fig. 10 | Accumulation of T cells and neutrophils negatively associates with GFR recovery in patients with AKI. **a** The estimated GFR (eGFR) was determined at reference, biopsy (AKI), and 6-month follow-up (6 m F/U). **b** Biopsy sections from each patient were immunofluorescence-stained with anti-CD3 ϵ (T-cell marker) and anti-megalin (PT marker, left panel) or anti-CD66b (PMN marker, right panel) and the percentage of nuclei positive for CD3 ϵ and CD66b calculated for all sections. Representative images of biopsies from a patient with full recovery [Case #0252, 150% recovery of GFR, magenta triangle in **a**], low-recovery [Case #0284, 52%

recovery of GFR, green square in **a**], and a healthy living donor are shown. Scale bars, 50 μ m. **c** Correlation between absolute eGFR increase (Δ eGFR) within 6 months after biopsy and T-cell infiltrate (%) or neutrophil infiltrate (%) at the time of AKI biopsy was determined by nonparametric Spearman correlation coefficient r . **d** Correlation between relative eGFR increase (fold change) within 6 months (6 m) after biopsy and T-cell infiltrate (%) or neutrophil infiltrate (%) at the time of biopsy was determined by nonparametric Spearman correlation coefficient r .

Cd74) and class I (*H2-D1* and *H2-K1*) genes, and thus become antigen-presenting cells capable of T-cell receptor (TCR) engagement with both Cd4+ and Cd8a+ T-cell activation⁴⁶. Consistent with this, *Lat*, which encodes the LAT adaptor protein component of the TCR activation complex, was significantly upregulated in intrarenal Cd4+ T cells (Supplemental Fig. 18a), and Cd8+ T cells were activated to express cytotoxins such as perforin, granzymes, and FAS ligand (Fig. 7c) following U-IRI. Interestingly, neutrophils that increase inflammatory cytokine and nitric oxide production have also been shown to efficiently interact with and prime naïve T cells directly or indirectly in vivo⁴⁷, suggesting that the simultaneous recruitment of both cell types beginning by day 7 after U-IRI may be important in promoting the secondary tubule injury as indicated by proximal tubule-*Vcam1* expression and collecting duct-*Lcn2* expression (Figs. 2 and 8c). This immune-mediated tubule injury appears to induce a different tubular response from the initial ischemic injury as *Havcr1* expression gradually decreased despite the tubular atrophy, whereas other injury markers such as *Vcam1* are upregulated only at this later stage of AKI to CKD transition. Consistent with this, a recent study by Kirita et al identified a distinct proinflammatory proximal tubule cell (FR-PTCs) state that fails to repair at the late stage of bilateral IRI⁴. These FR-PTCs were shown to increase *Vcam1* expression and were involved in positive regulation of lymphocyte activation⁴.

The question that our single-cell sequencing data raised is whether or not the late influx of T cells and neutrophils, occurring after proreparative macrophage activation has waned, is responsible for the late tubule dedifferentiation, sustained injury and atrophy seen following U-IRI. Experiments in which we selectively depleted either

T cells alone or neutrophils alone failed to reduce the progressive kidney and tubule atrophy (Supplemental Figs. 25 and 26), but when we depleted both T cells and neutrophils simultaneously there was a significant reduction in the degree of tubule atrophy following U-IRI with preservation of proximal tubule brush border and differentiation (Fig. 9). However, depletion of T cells and neutrophils did not fully prevent kidney atrophy when compared to the contralateral kidneys and control kidneys. This partial effect may be due to our inability to fully eliminate T-cell and neutrophil infiltration (~80% reduction based on immunostaining), or because administration of the anti-Thy1.2 and anti-Ly6G antibodies does not prevent accumulation of macrophages and DCs.

Alternatively, the partial response to T cell and PMN depletion may reflect the dichotomy of T-cell responses to kidney injury⁴⁸. It has been shown that CCR5 was upregulated in the CD3+ infiltrating T cells, and blockade of CCR5 using a neutralizing antibody in mice protected renal function after U-IRI⁴⁹. In addition, the store-operated calcium entry (SOCE) channel, *Orai1*, participates in the activation of Th17 cells and influences renal injury⁵⁰. Blockage of SOCE in rats attenuated Th17 cell activation, inflammation, and severity of AKI following IRI or intramuscular glycerol injection⁵⁰. In contrast, regulatory T (Treg) cells (TCR β +, CD4+, CD25+, Foxp3+) that infiltrate IRI kidneys during the healing process have been shown to promote kidney repair, likely by modulating proinflammatory cytokine production of other T-cell subsets⁵¹.

Finally, we show that patients who underwent a renal biopsy at the time of AKI exhibit a strong negative correlation between the number of infiltrating neutrophils and T cells present at the time of biopsy and

the subsequent recovery of estimated GFR (Fig. 10). While acknowledging the limitations of eGFR in patients with AKI, our findings are consistent with studies showing large numbers of terminally differentiated CD4+ T helper and CD8+ cytotoxic T cells in patients with ESRD⁵², and raise the ultimate question of whether or not these data may provide new targets for slowing or even preventing the progression from AKI to CKD in humans. By analyzing the chemokine-receptor interactions among cell types in the injured mouse kidneys, we identified several potentially important signaling interactions. For instance, interactions were identified between infiltrating macrophages and dendritic cells through CCL2-CCR2 signaling, and between macrophages, DC and T cells via CXCL16-CXCR6 signaling. We recently reported that blocking CCL2-CCR2 signaling by knock-out of *Ccr2* or use of the CCR2 antagonist RS102895 significantly reduced the number of macrophages, DCs and T cells following U-IRI, resulting in a reduction in ECM deposition and kidney injury marker expression²¹. However, the decrease in inflammatory cell numbers was modest in that study and there was no protection against kidney atrophy. It is perhaps not surprising that blocking a single pathway was ineffective given the complexity and redundancy built into inflammatory activation pathways, with alternative recruitment and activation signals such as CCL8/CCL6/CCL9/CCL5-CCR1 signaling identified between these same cell populations. Ultimately effective strategies may require targeting multiple inflammatory pathways and/or the initiation process that is likely mediated by the injured tubular and endothelial cells.

In summary, our results show that cross-talk between unrepaired tubular cells and macrophages, occurring after the initial reperfusion injury and associated first wave of neutrophil and macrophage infiltration has waned, promotes a second wave of inflammatory cell infiltration and activation that underlies the sustained tubule injury, dedifferentiation and atrophy seen after unilateral IRI. Macrophages appear to play a central role in recruiting the other immune cells, while the injured tubular cells themselves are primed to promote T-cell activation. The combined presence of neutrophils and activated T cells appears to be required for the subsequent tubule loss and kidney atrophy, suggesting that blocking their recruitment or activation may be a logical approach for suppressing AKI-to-CKD transition.

Limitations

There are some limitations in our studies. Despite our effort to optimize the dissociation method, the intrarenal cells including tubular epithelial cells, podocytes, endothelial cells, myofibroblast, immune cells might not be evenly dissociated from the injured kidneys as compared to controls. Hence, although the gene expression profiles and cell clustering should be highly accurate, the cell numbers of those populations in the scRNA-seq analyses may be impacted by these differences in cell disassociation.

Methods

Animal surgery and experimental protocol

All animal protocols were approved by the Yale University Animal Care and Use Committee (IACUC protocol number 10538). C57BL/6 (Envigo) wild-type mice (age 9–11 weeks) were used in this work. All mice were maintained on a 12-h light and 12-h dark cycle at the temperature between 68 and 79 °F and humidity between 30 and 70% with free access to standard food and water before and after surgery. Owing to the substantial difference in susceptibility to IRI injury between male and female mice⁵³, male mice were exclusively used to reduce total numbers of mice required for statistical analysis. Before surgery, all mice were subjected to anesthesia by intraperitoneal injection with ketamine (100 mg/kg) and xylazine (10 mg/kg) on a 37 °C warming pad. To establish the unilateral ischemia/reperfusion injury (U-IRI) model, the abdomen was opened, and warm renal ischemia was induced using a nontraumatic microaneurysm clip (FST Micro Clamps) on the left renal pedicle for 27 min, leaving the right kidney intact. To

establish the unilateral IRI with contralateral nephrectomy (IRI/CL-NX) model, the right kidney was surgically removed at the time of left kidney ischemia. During surgery, all mice received intraperitoneal phosphate-buffered saline (PBS) and buprenorphine (0.1 mg/kg) to avoid dehydration and postoperative pain, respectively. The mice were sacrificed on day 1, 7, 14, and 30 after U-IRI or IRI/CL-NX ($n = 10$ mice/end point). Baseline control mice were sacrificed and denoted as day 0 for the injury ($n = 10$ mice) or at day 30 and designated as age-matched controls ($n = 10$). To establish the nephrectomy (NX) alone model, the right kidney was surgically removed, and the mice were sacrificed on day 30 after NX ($n = 8$). Additional mice were sacrificed on day 7, 14, and 30 after U-IRI or IRI/CL-NX ($n = 2$ mice at each time point/model and 2 healthy control mice) for kidney cell isolation followed by single-cell RNA sequencing. Blood and tissue samples were obtained at the indicated times after the surgery. Serum creatinine and blood urea nitrogen (BUN) were measured at the Yale George M. O'Brien Kidney Center.

In vivo depletion of T cells and neutrophils

To deplete T cells and neutrophils, wild-type mice were i.p. injected with 200 μ g anti-mouse Thy1.2 (CD90.2) antibody (clone 30H12, BioXCell) once in 3 days and 200 μ g anti-mouse Ly6G (clone 1A8, BioXCell) ($n = 9$ mice) every other day or PBS control ($n = 9$ mice) starting on day 5 after U-IRI. The depletion efficacy was confirmed at the kidney level using immunohistochemistry against CD3 ϵ , CD4, CD8 α , and Ly6G, respectively, and qPCR analysis for *Cd3e*, *Cd4*, *Cd8a*, and *Ly6g*, respectively, on the whole-kidney RNA at the end point (day 30 after U-IRI).

ELISA of serum KIM-1 and NGAL levels

Serum KIM1 and NGAL concentrations were measured using mouse TIM-1/KIM-1/HAVCR and Lipocalin-2/NGAL quantikine ELISA kits (R&D Systems) according to the manufacturer's instructions.

Preparation of single-cell suspension

Euthanized mice were perfused with chilled 3 \times PBS (10 mL) via the left ventricle. Kidneys were harvested, minced into ~ 1 mm³ cubes, and digested using LiberaseTM (100 μ g/mL) and DNase I (10 μ g/mL) (Roche Diagnostics) for 25 min at 37 °C. Reaction was deactivated by adding chilled DMEM with 10% FBS. The solution was then passed through a 40- μ m cell strainer. After centrifugation at 300 $\times g$ for 10 min at 4 °C, the cell pellet was resuspended in chilled DMEM with 10% FBS and passed through another 40- μ m cell strainer. The dead cells were removed using Dead Cell Removal Kit (Miltenyi Biotec). Cell number and viability were analyzed using trypan blue staining (Invitrogen). This method generated single-cell suspensions with greater than 80% viability.

Single-cell-RNA-sequencing (scRNA-seq) library generation and sequencing

scRNA-seq library and sequencing were performed at the Yale Center for Genome Analysis (YCGA). Briefly, single cells, reagents and a single Gel Bead containing barcoded oligonucleotides were encapsulated into nanoliter-sized Gel Bead in Emulsion (GEM) using the GemCodeTM Technology 10x Genomics. Lysis and barcoded reverse transcription of polyadenylated mRNA from single cells were performed inside each GEM. The scRNA-seq libraries were finished in single bulk reaction. The cDNA libraries were constructed using the 10x ChromiumTM Single-cell 3' Library Kit. Qualitative analysis was performed using the Agilent Bioanalyzer High Sensitivity DNA assay as shown in Supplementary Fig. 24. The final libraries from IRI/CL-NX and U-IRI kidneys were sequenced on an Illumina HiSeq 4000 sequencer. Cell Ranger version 5.0.1 was used to process Chromium single-cell 3' RNA-seq output and align the Read to the mouse reference transcriptome (mm10-2020-A), all of which were provided by the YCGA.

scRNA-seq data analysis

Downstream data analysis was performed using the Seurat v4.0 R package. The Seurat integration strategy was performed to identify common cell types and enable comparative analyses between IRI/CL-NX and U-IRI kidneys at each time point^{54,55}. Briefly, all the datasets were first merged for the quality control (QC) analysis. Poor quality cells with <200 unique genes and <500 unique molecular identifier (UMI) counts (likely cell fragment) and >100,000 UMI (potentially cell duplet) were excluded. Cells were excluded if their mitochondrial gene percentages were over 50%. Low-complexity cells like red blood cells with <0.8 log10 genes per UMI counts were also excluded⁵⁶. Only genes expressed in 5 or more cells were used for further analysis. The QC filters resulted in a total of 95,343 cells with a median of 2743 UMI counts per cell at a sequencing depth of 44,719 genes across 95,343 cells. The merged dataset was split, normalized, cell cycle scored, SCTransformed, and integrated using integrated anchors⁵⁷. Confounding sources of variation including mitochondrial gene content were removed for downstream clustering analysis.

Principle component analysis (PCA) was performed on the scaled data. The top 20 principal components were chosen for cell clustering and neighbors finding with $k_{\text{param}} = 20$, perplexity of 30, and resolution = 0.8. The Uniform Manifold Approximation and Projection (UMAP) was used to visualize the single cells in two-dimensional space. Each cluster was screened for marker genes by differential expression analysis based on the non-parametric Wilcoxon rank sum test for all clusters with genes expressed in at least 25% of cells either inside or outside of a cluster. Based on the kidney cell and immune cell lineage-specific marker expression, eighteen cell clusters were identified. Both IRI/CL-NX and U-IRI datasets at each time point could be split from the integrated dataset for differential analyses. The average expression of both IRI/CL-NX and U-IRI cells was plotted on using volcano plots. The outliers were used to identify the genes that were differentially expressed between the models in each cluster. All the changes in gene expression were visualized in dot plots or volcano plots. Gene set enrichment analyses were performed using the ClusterProfiler and Gene Ontology (GO) Resource⁵⁸. The potential ligand-receptor interaction analyses were performed using the NicheNet R package^{30,31} by linking potential ligands expressed by sender cells to their target genes that were differentially expressed by receiver cells and their corresponding receptors. The ligand-receptor pairings for each cell type were visualized by a chord diagram using the R package *circize*⁵⁹.

Quantitative PCR analysis

Whole-kidney RNA was extracted with an RNeasy Mini kit (Qiagen) and reverse transcribed using the iScript cDNA Synthesis Kit (Bio-Rad). Gene expression analysis was determined by quantitative real-time PCR using an iCycler iQ (Bio-Rad) and normalized to hypoxanthine-guanine phosphoribosyltransferase (*Hprt*). The primers included previously published sequences²¹, and those provided in Supplementary Table 9. The data were expressed using the comparative threshold cycle (ΔCT) method, and the mRNA ratios were given by $2^{-\Delta\text{CT}}$.

Immunohistochemistry (IHC) and immunofluorescence (IF)

Kidneys were fixed in 10% neutral-buffered formalin and embedded in paraffin. Deparaffinized kidney sections were rehydrated in graded alcohols (100%, 95%, 90%, 80%, and 70%) and microwaved in citrate buffer antigen retrieval for 20 min. Endogenous peroxidase activity quenched by incubation in 3% (vol/vol) H_2O_2 for 15 min. The sections were incubated overnight at 4 °C with the primary antibody. After washing with TBST, the sections were incubated with biotinylated secondary antibody (Vector Laboratories) followed by VECTASTAIN Elite ABC system (Vector Laboratories). DAB (Vector Laboratories) and hematoxylin (Vector Laboratories) were used as the chromogen and the nuclear counterstain, respectively. The primary antibodies were

omitted as negative controls. Primary antibodies were as follows: F4/80, CD11c, Ly6G, CD3e, CD4, CD8 α (#70076, #97585, #87048 S, #99940, #25229, and #98941; Cell Signaling Technology, respectively, 1:100 dilution) and primary rabbit polyclonal antibody against megalin (anti-MC220⁶⁰ original obtained from Dr. Daniel Biemesderfer, Yale Section of Nephrology). Lotus tetragonolobus lectin (LTL) was detected by IHC using primary antibodies against biotinylated LTL (#B-1325, Vector Laboratories, 1:200 dilution). All the IHC staining slides were scanned using Aperio LV1 Real-time slide scanner and processed using ImageScope software. Six independent fields in cortex and four independent fields in outer medulla were analyzed per kidney section. The percent area of F4/80-, CD11c-, Ly6G-, CD3e-, CD4-, and CD8 α -positive staining was quantified using IHC Profiler in ImageJ (NIH).

Kidney-specific cadherin (KSP-Cadherin) and UMOD were detected by IF using primary antibodies against UMOD (#sc-20631, Santa Cruz Biotechnology, 1:100 dilution) and primary mouse monoclonal antibody against KSP-Cadherin (clone:4H6/F6²⁴, kindly provided by Dr. Robert Brent Thomson, Yale Section of Nephrology, 1:100 dilution). All the IF staining slides were scanned by Panoramic 250 FLASH III (iHisto Inc, MA), and the images were processed using CaseViewer software. Megalin and KIM-1 were detected by IF using primary antibodies against megalin (anti-MC220⁶⁰, 1:100 dilution) and TIM-1/KIM-1/HAVCR (#AF1817, Novus Biologicals, 1:100 dilution)⁶¹. Six to ten random fields in cortex were imaged per kidney section. The percent area of megalin and KIM-1-positive staining was quantified using ImageJ.

Confocal microscopy

Three mice were sacrificed 14 days after U-IRI. The kidneys were perfused with 4% paraformaldehyde (PFA) and embedded in optimum cutting temperature (OCT) compound (Tissue Tek). Kidneys were cryosectioned at 5 μm thickness and mounted on Superfrost slides. Sections were washed with PBS, blocked with 10% normal donkey serum, and then stained with primary antibodies against F4/80 (#MCA497GA, Clone:A3-1, Bio-Rad, 1:100 dilution) and Ly6G or CD3e (#87048 S and #99940, Cell Signaling Technology, 1:100 dilution). The sections were mounted with VECTASHIELD® HardSet™ Antifade Mounting Medium with DAPI (4,6-diamidino-2-phenylindole). The fluorescence images were obtained by confocal microscopy (Zeiss LSM 880).

Western blot analysis

Kidney lysates were fractionated using a RIPA lysis and extraction buffer (Thermo Fisher Scientific) fixed with cOmplete, EDTA-free, protease inhibitor (Roche). Protein concentration was measured using Bio-Rad Protein Assay. Fifty micrograms of protein was separated by SDS electrophoresis using 7.5% polyacrylamide gel and transferred to an Immobilon PVDF membrane (Millipore). Membrane was blocked with 5% non-fat milk in TBST for 2 hrs and probed overnight at 4 °C with the primary antibody against TIM-1/KIM-1/HAVCR (#AF1817, Novus Biologicals). After washing the membrane with TBST, it was incubated for 1 h at room temperature with HRP-conjugated secondary antibody (Thermo Fisher Scientific). The membrane was developed using the ECL Detection System (Thermo Fisher Scientific) and imaged using the Odyssey Fc Imaging System (LI-COR Biosciences). Next, the membrane was washed with TBS and then immersed and incubated in Restore™ PLUS Western Blot Stripping Buffer (Thermo Fisher Scientific) for 15 min. After TBST wash, the same membrane was blocked with 5% non-fat milk in TBST for 2 hrs and probed overnight at 4 °C with the primary antibody against GAPDH (HRP Conjugate) (#51332; Cell Signaling Technology). The membrane was developed using the ECL Detection System and exposed to autoradiographic films. The films were scanned on an Epson Perfection V500 Photo Scanner. Densitometry was analyzed using ImageJ. The uncropped scans of all blots were supplied in the Source Data files.

Human kidney biopsy

Human kidney biopsy samples were obtained in accordance with the policies of Yale University's Human Investigations Committee (HIC approval number 11110009286). Written informed consent for research use of patient samples was obtained from each patient by study team. Living donor kidney biopsies were collected under a protocol approved by the Yale University institutional review board (Protocol 2000022915). Informed consent was obtained for all patients before enrollment. Following organ harvest, an 18-gauge core or wedge biopsy was collected intraoperatively prior to organ transplantation^{36,62}. No compensation was provided for the study participation. The banked AKI samples obtained between 2015 and 2018 were acquired retrospectively after chart review. All data were deidentified and maintained on a secure database. We estimated GFR (eGFR) using the CKD-epidemiology equation⁶³. Ten cases were identified using the following criteria: baseline eGFR ≥ 60 mL/min/1.73 m², presence of AKI, exclusion of those with GN, DKD, or AIN, availability of biopsy sample, and availability of 6-month follow-up eGFR (8/10 with pathologic diagnosis of ATI, acute tubular injury). CD3 ϵ - and CD66b-cells were detected by IF using primary monoclonal antibodies against CD3 ϵ (#NBP2-53387, Novus Biologicals, 1:100 dilution) and CD66b (#305102, BioLegend, 1:100 dilution), respectively, and proximal tubules were visualized by IF using polyclonal antibody against LRP2 (#19700-1-AP, Thermo Fisher Scientific, 1:100 dilution) to identify renal cortical regions on the biopsy specimen. All the IF staining sections were tile-scanned by Zeiss LSM 880 with Airyscan Microscope at the Yale Center for Advanced Light Microscopy Facility, and the images were processed using Zeiss Zen lite software. The number of T cells and neutrophils in the entire sample cortex were counted in a blinded manner and normalized to the total number of cells (identified by DAPI + nuclei) in the same cortical region.

Statistical analysis

The data were expressed as means \pm standard deviation (SD). Two-group comparison was performed by Student *t*-test. Multigroup comparison was performed by one-way analysis of variance (ANOVA) for group mean comparison followed by Tukey's multiple comparison test for subgroup comparison. Two-group time-course comparison was performed by two-way ANOVA for model comparison to test whether there is a difference between the models and in the time-course, followed by Bonferroni post-tests or Tukey's post-tests for subgroup comparison (Supplementary Tables 1 and 3). Correlation of gene expression was performed by Pearson correlation coefficient *r* with two-tailed *p*-value (Supplementary Tables 4–6). Correlation of T cells/neutrophils and eGFR was performed by nonparametric Spearman correlation coefficient *r* with two-tailed *p*-value. All the statistical analysis was performed using Prism 8 (GraphPad Software). A value of *p* < 0.05 was considered statistically significant.

Reporting summary

Further information on research design is available in the Nature Research Reporting Summary linked to this article.

Data availability

The scRNA-sequencing data generated in this study have been deposited and publicly available in the GEO database under accession code [GSE197626](https://www.ncbi.nlm.nih.gov/geo/query/acc.cgi?acc=GSE197626). Source data are provided with this paper as a Source Data file. The remaining data are available within the Article or from the authors upon request. Source data are provided with this paper.

Code availability

The analysis code has been deposited and publicly available in Zenodo at <https://zenodo.org/record/6794806#.YsL9AnaZMuU> or from the authors upon request.

References

- Zuk, A. & Bonventre, J. V. Recent advances in acute kidney injury and its consequences and impact on chronic kidney disease. *Curr. Opin. Nephrol. Hypertens.* **28**, 397–405 (2019).
- Wilflingseder, J. et al. Enhancer and super-enhancer dynamics in repair after ischemic acute kidney injury. *Nat. Commun.* **11**, 3383 (2020).
- Chang-Panesso, M. & Humphreys, B. D. Cellular plasticity in kidney injury and repair. *Nat. Rev. Nephrol.* **13**, 39–46 (2017).
- Kirita, Y., Wu, H., Uchimura, K., Wilson, P. C. & Humphreys, B. D. Cell profiling of mouse acute kidney injury reveals conserved cellular responses to injury. *Proc. Natl Acad. Sci. USA* **117**, 15874–15883 (2020).
- He, L. et al. AKI on CKD: heightened injury, suppressed repair, and the underlying mechanisms. *Kidney Int.* **92**, 1071–1083 (2017).
- Huen, S. C. & Cantley, L. G. Macrophages in renal injury and repair. *Annu. Rev. Physiol.* **79**, 449–469 (2017).
- Lee, S. et al. Distinct macrophage phenotypes contribute to kidney injury and repair. *J. Am. Soc. Nephrol.* **22**, 317–326 (2011).
- Perry, H. M. & Okusa, M. D. Driving change: kidney proximal tubule CSF-1 polarizes macrophages. *Kidney Int.* **88**, 1219–1221 (2015).
- Palmer, M. B., Vichot, A. A., Cantley, L. G. & Moeckel, G. W. Quantification and localization of M2 macrophages in human kidneys with acute tubular injury. *Int. J. Nephrol. Renovasc. Dis.* **7**, 415–419 (2014).
- Wang, Y. et al. Proximal tubule-derived colony stimulating factor-1 mediates polarization of renal macrophages and dendritic cells, and recovery in acute kidney injury. *Kidney Int.* **88**, 1274–1282 (2015).
- Basile, D. P. et al. Progression after AKI: understanding maladaptive repair processes to predict and identify therapeutic treatments. *J. Am. Soc. Nephrol.* **27**, 687–697 (2016).
- Chawla, L. S. & Kimmel, P. L. Acute kidney injury and chronic kidney disease: an integrated clinical syndrome. *Kidney Int.* **82**, 516–524 (2012).
- Coca, S. G., Singanamala, S. & Parikh, C. R. Chronic kidney disease after acute kidney injury: a systematic review and meta-analysis. *Kidney Int.* **81**, 442–448 (2012).
- Ikizler, T. A. et al. A prospective cohort study of acute kidney injury and kidney outcomes, cardiovascular events, and death. *Kidney Int.* **99**, 456–465 (2020).
- Lin, S. L., Castano, A. P., Nowlin, B. T., Lupher, M. L. Jr. & Duffield, J. S. Bone marrow Ly6Chigh monocytes are selectively recruited to injured kidney and differentiate into functionally distinct populations. *J. Immunol.* **183**, 6733–6743 (2009).
- Xavier, S. et al. Pericytes and immune cells contribute to complement activation in tubulointerstitial fibrosis. *Am. J. Physiol. Ren. Physiol.* **312**, F516–F532 (2017).
- Huen, S. C., Moeckel, G. W. & Cantley, L. G. Macrophage-specific deletion of transforming growth factor- β 1 does not prevent renal fibrosis after severe ischemia-reperfusion or obstructive injury. *Am. J. Physiol. Ren. Physiol.* **305**, F477–F484 (2013).
- Kim, M. G. et al. The role of M2 macrophages in the progression of chronic kidney disease following acute kidney injury. *PLoS ONE* **10**, e0143961 (2015).
- Le Clef, N., Verhulst, A., D'Haese, P. C. & Vervaeke, B. A. Unilateral renal ischemia-reperfusion as a robust model for acute to chronic kidney injury in mice. *PLoS ONE* **11**, e0152153 (2016).
- Montgomery, T. A. et al. Breast regression protein-39/chitinase 3-like 1 promotes renal fibrosis after kidney injury via activation of myofibroblasts. *J. Am. Soc. Nephrol.* **28**, 3218–3226 (2017).
- Xu, L., Sharkey, D. & Cantley, L. G. Tubular GM-CSF promotes late MCP-1/CCR2-mediated fibrosis and inflammation after ischemia/reperfusion injury. *J. Am. Soc. Nephrol.* **30**, 1825–1840 (2019).

22. Venkatachalam, M. A., Weinberg, J. M., Kriz, W. & Bidani, A. K. Failed tubule recovery, AKI-CKD transition, and kidney disease progression. *J. Am. Soc. Nephrol.* **26**, 1765–1776 (2015).
23. Thomson, R. B. et al. Isolation and cDNA cloning of Ksp-cadherin, a novel kidney-specific member of the cadherin multigene family. *J. Biol. Chem.* **270**, 17594–17601 (1995).
24. Thomson, R. B. et al. cDNA cloning and chromosomal localization of the human and mouse isoforms of Ksp-cadherin. *Genomics* **51**, 445–451 (1998).
25. Baisantray, A. et al. Autophagy induces prosenescent changes in proximal tubular S3 segments. *J. Am. Soc. Nephrol.* **27**, 1609–1616 (2016).
26. Ide, N. et al. In vivo evidence for a limited role of proximal tubular Klotho in renal phosphate handling. *Kidney Int.* **90**, 348–362 (2016).
27. Kiryluk, K. et al. Precision medicine for acute kidney injury (AKI): redefining AKI by agnostic kidney tissue interrogation and genetics. *Semin. Nephrol.* **38**, 40–51 (2018).
28. Shin, N. S. et al. Arginase-1 is required for macrophage-mediated renal tubule regeneration. *J. Am. Soc. Nephrol.* **33**, 1077–1086 (2022).
29. Puthumana, J. et al. Biomarkers of inflammation and repair in kidney disease progression. *J. Clin. Invest.* **131**, e139927 (2020).
30. Browaeys, R., Saelens, W. & Saeys, Y. NicheNet: modeling inter-cellular communication by linking ligands to target genes. *Nat. Methods* **17**, 159–162 (2020).
31. Bonnardel, J. et al. Stellate cells, hepatocytes, and endothelial cells imprint the kupffer cell identity on monocytes colonizing the liver macrophage niche. *Immunity* **51**, 638–654.e639 (2019).
32. Lu, L. et al. Depletion of macrophages and dendritic cells in ischemic acute kidney injury. *Am. J. Nephrol.* **35**, 181–190 (2012).
33. Kinsey, G. R., Li, L. & Okusa, M. D. Inflammation in acute kidney injury. *Nephron Exp. Nephrol.* **109**, e102–e107 (2008).
34. Moledina, D. G. et al. Urine TNF- α and IL-9 for clinical diagnosis of acute interstitial nephritis. *JCI Insight* **4**, e127456 (2019).
35. Moledina, D. G. et al. Urine interleukin-9 and tumor necrosis factor- α for prognosis of human acute interstitial nephritis. *Nephrol. Dial. Transplant* **36**, 1851–1858 (2020).
36. Singh, N. et al. Development of a 2-dimensional atlas of the human kidney with imaging mass cytometry. *JCI Insight* **4**, e129477 (2019).
37. Schmidt, I. M. et al. Chitinase-like protein Brp-39/YKL-40 modulates the renal response to ischemic injury and predicts delayed allograft function. *J. Am. Soc. Nephrol.* **24**, 309–319 (2013).
38. Yang, L. et al. KIM-1-mediated phagocytosis reduces acute injury to the kidney. *J. Clin. Invest.* **125**, 1620–1636 (2015).
39. Song, J. et al. Characterization and fate of telomerase-expressing epithelia during kidney repair. *J. Am. Soc. Nephrol.* **22**, 2256–2265 (2011).
40. Inoue, T. et al. Vagus nerve stimulation mediates protection from kidney ischemia-reperfusion injury through α 7nAChR⁺ splenocytes. *J. Clin. Invest.* **126**, 1939–1952 (2016).
41. Liu, J. et al. Molecular characterization of the transition from acute to chronic kidney injury following ischemia/reperfusion. *JCI Insight* **2**, e94716 (2017).
42. Karasawa, K. et al. Vascular-resident CD169-positive monocytes and macrophages control neutrophil accumulation in the kidney with ischemia-reperfusion injury. *J. Am. Soc. Nephrol.* **26**, 896–906 (2015).
43. Burne-Taney, M. J. et al. Transfer of lymphocytes from mice with renal ischemia can induce albuminuria in naive mice: a possible mechanism linking early injury and progressive renal disease? *Am. J. Physiol. Ren. Physiol.* **291**, F981–F986 (2006).
44. Basile, D. P., Leonard, E. C., Tonade, D., Friedrich, J. L. & Goenka, S. Distinct effects on long-term function of injured and contralateral kidneys following unilateral renal ischemia-reperfusion. *Am. J. Physiol. Ren. Physiol.* **302**, F625–F635 (2012).
45. Ascon, M. et al. Renal ischemia-reperfusion leads to long term infiltration of activated and effector-memory T lymphocytes. *Kidney Int.* **75**, 526–535 (2009).
46. Satpute, S. R. et al. The role for T cell repertoire/antigen-specific interactions in experimental kidney ischemia reperfusion injury. *J. Immunol.* **183**, 984–992 (2009).
47. Beauvillain, C. et al. Neutrophils efficiently cross-prime naive T cells in vivo. *Blood* **110**, 2965–2973 (2007).
48. Rabb, H. The T cell as a bridge between innate and adaptive immune systems: implications for the kidney. *Kidney Int.* **61**, 1935–1946 (2002).
49. Ko, G. J. et al. Transcriptional analysis of infiltrating T cells in kidney ischemia-reperfusion injury reveals a pathophysiological role for CCR5. *Am. J. Physiol. Ren. Physiol.* **302**, F762–F773 (2012).
50. Mehrotra, P., Sturek, M., Neyra, J. A. & Basile, D. P. Calcium channel Orai1 promotes lymphocyte IL-17 expression and progressive kidney injury. *J. Clin. Invest.* **130**, 1052 (2020).
51. Gandolfo, M. T. et al. Foxp3⁺ regulatory T cells participate in repair of ischemic acute kidney injury. *Kidney Int.* **76**, 717–729 (2009).
52. Betjes, M. G. Immune cell dysfunction and inflammation in end-stage renal disease. *Nat. Rev. Nephrol.* **9**, 255–265 (2013).
53. Wei, Q. & Dong, Z. Mouse model of ischemic acute kidney injury: technical notes and tricks. *Am. J. Physiol. Ren. Physiol.* **303**, F1487–F1494 (2012).
54. Butler, A., Hoffman, P., Smibert, P., Papalexis, E. & Satija, R. Integrating single-cell transcriptomic data across different conditions, technologies, and species. *Nat. Biotechnol.* **36**, 411–420 (2018).
55. Kang, H. M. et al. Multiplexed droplet single-cell RNA-sequencing using natural genetic variation. *Nat. Biotechnol.* **36**, 89–94 (2018).
56. Bassez, A. et al. A single-cell map of intratumoral changes during anti-PD1 treatment of patients with breast cancer. *Nat. Med.* **27**, 820–832 (2021).
57. Hafemeister, C. & Satija, R. Normalization and variance stabilization of single-cell RNA-seq data using regularized negative binomial regression. *Genome Biol.* **20**, 296 (2019).
58. Yu, G., Wang, L.-G., Han, Y. & He, Q.-Y. clusterProfiler: an R package for comparing biological themes among gene clusters. *OmicS: J. Integr. Biol.* **16**, 284–287 (2012).
59. Gu, Z., Gu, L., Eils, R., Schlesner, M. & Brors, B. circlize Implements and enhances circular visualization in R. *Bioinformatics* **30**, 2811–2812 (2014).
60. Zou, Z. et al. Linking receptor-mediated endocytosis and cell signaling: evidence for regulated intramembrane proteolysis of megalin in proximal tubule. *J. Biol. Chem.* **279**, 34302–34310 (2004).
61. Chang-Panesso, M. et al. FOXM1 drives proximal tubule proliferation during repair from acute ischemic kidney injury. *J. Clin. Invest.* **129**, 5501–5517 (2019).
62. Avigan, Z. M. et al. Tubular cell dropout in preimplantation deceased donor biopsies as a predictor of delayed graft function. *Transpl. Direct* **7**, e716 (2021).
63. Levey, A. S. et al. A new equation to estimate glomerular filtration rate. *Ann. Intern. Med.* **150**, 604–612 (2009).

Acknowledgements

We are grateful to Dr. Joseph Craft from the Section of Rheumatology at the Yale School of Medicine for providing advice in T-cell depletion and Robert Brent Thomson for providing the primary antibody against mouse KSP-Cadherin. This work was supported by National Institutes of Health Grant T32 DK007276 and K01 DK120783 (to L.X.), R01 DK093771 (to L.G.C.), K23 DK117065 (to D.G.M.), P30 DK079310 (George M. O'Brien Kidney Center at Yale), and S10 OD023598 (Yale Center for Advanced Light Microscopy Facility).

Author contributions

L.X. designed and performed the primary experiments, analyzed the data, and wrote the manuscript. J.G. in part performed single-cell preparation, data interpretation, and edited manuscript. D.G.M. obtained human samples, performed patient chart review, and edited the manuscript. L.G.C. oversaw the project and edited the manuscript.

Competing interests

The authors declare no competing interests.

Additional information

Supplementary information The online version contains supplementary material available at <https://doi.org/10.1038/s41467-022-32634-0>.

Correspondence and requests for materials should be addressed to Leyuan Xu or Lloyd G. Cantley.

Peer review information *Nature Communications* thanks Rajasree Menon and the other, anonymous, reviewer(s) for their contribution to the peer review of this work.

Reprints and permission information is available at <http://www.nature.com/reprints>

Publisher's note Springer Nature remains neutral with regard to jurisdictional claims in published maps and institutional affiliations.

Open Access This article is licensed under a Creative Commons Attribution 4.0 International License, which permits use, sharing, adaptation, distribution and reproduction in any medium or format, as long as you give appropriate credit to the original author(s) and the source, provide a link to the Creative Commons license, and indicate if changes were made. The images or other third party material in this article are included in the article's Creative Commons license, unless indicated otherwise in a credit line to the material. If material is not included in the article's Creative Commons license and your intended use is not permitted by statutory regulation or exceeds the permitted use, you will need to obtain permission directly from the copyright holder. To view a copy of this license, visit <http://creativecommons.org/licenses/by/4.0/>.

© The Author(s) 2022